INDOCYANINE GREEN LOADED POLY(LACTIC ACID) NANOPARTICLES MEDIATED PHOTOTHERAPY OF CANCER

by

Melike Güney Akkurt

B.S., in Biomedical Engineering, Yeditepe University, 2009

M.S., in Biomedical Engineering, Boğaziçi University, 2014

Submitted to the Institute of Biomedical Engineering

in partial fulfillment of the requirements

for the degree of

Doctor

of

Philosophy

Boğaziçi University

2022

ACKNOWLEDGMENTS

I would like to express my sincerest gratitude to my advisor Prof. Murat Gülsoy for his guidance throughout my entire postgraduate education. I also wish to show my appreciation to the members of my PhD committee; Professors İnci Çilesiz, Murat Kazancı, Bora Garipcan and Banu İyisan for their valuable insights and contributions.

I wish to extend my special thanks to fellow members of Biophotonics Laboratory, Burcu Güleryüz and Ayşe Işık for their help during this project, as well as all other members for their valuable contributions.

This project was funded by Boğaziçi University Research Fund Grant Number 12321.

ACADEMIC ETHICS AND INTEGRITY STATEMENT

I, Melike Güney Akkurt, hereby certify that I am aware of the Academic Ethics and Integrity Policy issued by the Council of Higher Education (YÖK) and I fully acknowledge all the consequences due to its violation by plagiarism or any other way.

Name :

Signature:

Date:

ABSTRACT

INDOCYANINE GREEN LOADED POLY(LACTIC ACID) NANOPARTICLES MEDIATED PHOTOTHERAPY OF CANCER

Phototherapy is a promising approach for cancer treatment which can be utilized alone or in combination with other treatment modalities. Among the available photosensitizers for phototherapy, indocyanine green (ICG) merits special attention, owing to its near infrared absorption characteristics and low dark toxicity. However, a strong tendency for protein-binding and aggregate-forming limits its use as a phototherapeutic agent. Such a drawback can be eliminated with the utilization of nano-sized drug delivery systems to encapsulate and protect ICG molecules. Numerous drug delivery systems incorporating ICG for phototherapeutic or imaging purposes are reported in the literature. However; these systems mostly contain other therapeutic agents as well, making it difficult to assess the effects of ICG alone. Hence, this study was aimed to explore the impact of only-ICG encapsulating polymeric nanoparticles as a phototherapeutic agent. Poly(lactic acid) nanoparticles produced via a single-step nanoprecipitation method for encapsulation and delivery of ICG molecules were used to this end and their phototherapeutic effects on prostate cancer cells were examined. This study demonstrated that ICG-encapsulating poly(lactic acid) nanoparticles could be utilized as a phototherapeutic agent in order to inhibit cellular viability on prostate cancer cells and that the decrease in cell viability was primarily due to photothermal effect.

Keywords: Anticancer Phototherapy, Photodynamic Therapy, Photothermal Therapy, Indocyanine Green,Polymeric Nanoparticles, Nanoprecipitation.

ÖZET

İNDOSİYANİN YEŞİLİ YÜKLÜ POLİ(LAKTİK ASİT) NANOPARTİKÜL ARACILI KANSER FOTOTERAPİSİ

Fototerapi, kanser tedavisinde tek başına veya diğer tedavi yöntemleri ile birlikte uygulanabilen umut vaadeden bir yaklaşımdır. Fototerapi için mevcut fotosensitizanlar arasında indosiyanin yeşili (ICG), yakın kızılötesi absorpsiyon özellikleri ve düşük karanlık toksisitesi nedeniyle özel ilgiyi hak etmektedir. Bununla birlikte, proteinlere bağlanma ve kümelenmeye yönelik güçlü bir eğilim göstermesi fototerapötik bir ajan olarak kullanımını kısıtlamaktadır. Bu dezavantaj, ICG moleküllerini kapsüllemek ve korumak için nano boyutlu ilaç taşıma sisteminin kullanılmasıyla ortadan kaldırılabilir. Literatürde fototerapötik veya görüntüleme amaçlı ICG içeren çeşitli ilaç taşıma sistemleri rapor edilmiştir. Ancak bu sistemlerin çoğunlukla diğer terapötik ajanları da içermesi, sadece ICG'nin etkilerini değerlendirmeyi zorlaştırmaktadır. Dolayısıyla bu çalışmanın amacı, fototerapötik bir ajan olarak sadece ICG taşıyan polimerik nanoparça-cıkların etkisini araştırmaktır. Bu amaçla tek aşamalı bir nanoçökeltme yöntemiyle üretilen poli(laktik asit) nanoparçacıklar ICG moleküllerinin kapsüllenmesi ve taşınması için kullanılmış ve prostat kanseri hücreleri üzerindeki fototerapötik etkileri incelenmiştir. Bu çalışma, ICG-kapsülleyen poli(laktik asit) nanoparçacıkların prostat kanseri hücrelerinde hücresel canlılığın inhibisyonu için bir fototerapötik ajan olarak kullanılabileceğini ve hücre canlılığındaki azalmanın öncelikle fototermal etkiden kaynaklandığını göstermiştir.

Keywords: Antikanser Fototerapi, Fotodinamik Terapi, Fototermal Terapi, İndosiyanin Yeşili, Polimerik Nanoparçacıklar, Nanopresipitasyon.

TABLE OF CONTENTS

LIST OF FIGURES

LIST OF TABLES

LIST OF SYMBOLS

μM	Micromolar
μs	Microsecond
mM	Millimolar
C	Concentration
J	Joule
W	Watt
$^1O_2$	Singlet Oxygen
°C	Degrees Celcius
Φ_{ST}	Quantum Yield of Transition from Singlet to Triplet State
μ_a	Absorption Coefficient

LIST OF ABBREVIATIONS

ANOVA	Analysis of Variance
CP	Carboplatin
DCM	Dichloromethane
DDS	Drug Delivery System
DLS	Dynamic Light Scattering
DMSO	Dimethyl sulfoxide
DPBF	1,3-diphenylisobenzofuran
DTX	Docetaxel
EPR	Enhanced Permeability and Retention
FBS	Fetal Bovine Serum
FDA	U.S. Food and Drug Administration
ICG	Indocyanine Green
ICGNP	Indocyanine Green Nanoparticles
MPS	Mononuclear Phagocytic System
MTT	3-(4,5-dimethylthiazol-2-yl)-2,5-diphenyltetrazolium bromide
NIR	Near Infrared
PBS	Phosphate Buffered Saline
PCL	Polycaprolactone
PDI	Polydispersity Index
PDT	Photodynamic Therapy
PLA	Poly(lactic acid)
PLGA	poly(lactic-co-glycolic acid)
PS	Photosensitizer
PTT	Photothermal Therapy
ROS	Reactive Oxygen Species
R848	Resiquimod
S/NS	Solvent/non-solvent ratio
SEM	Scanning electron microscopy

STEM	Scanning transmission electron microscopy
%EE	%Encapsulation Efficiency
%LC	%Loading Capacity

1. INTRODUCTION

1.1 Motivation

Oncological phototherapy is a hypernym that includes photodynamic therapy (PDT), photothermal therapy (PTT) and photoactivated chemotherapy (PACT), in which light is utilized in conjunction with a chemical to treat tumors. All these treatment modalities display favorable characteristics such as; low invasiveness,accurate cancer targeting that minimizes damage to healthy tissues, and little or no cross-resistance with other cancer treatments which enables combination treatments [1]. Although the therapeutic use of light was well-known and utilized throughout human history, effects of photodynamic action by external sensitizer administration were introduced into modern scientific literature in the beginning of 20^{th} century. von Tappeiner and Raab's works on several photosensitizing agents on various lesions ignited an interest in the mechanisms of action as well as the therapeutic potential of PDT and PTT [2,3].

Initially, research on phototherapeutic methods for cancer treatment had started as identification and synthesis of various photosensitizer molecules as well as development of novel illumination techniques. Towards the end of the century, with the advancements in nanotechnology, nano-sized drug carriers for photosensitizers were introduced. These nanocarriers rapidly evolved into multi-purpose anticancer platforms with imaging and targeting capabilities that incorporate photosensitizers along with chemotherapeutic agents, inspiring a completely new research area [4–6].

Amongst the various sensitizing agents utilized in such platforms, indocyanine green (ICG) merits special attention. ICG is an FDA-approved diagnostic near-infrared (NIR)dye that has been studied extensively as a photosensitizer [7–16]. ICG exhibits very low dark toxicity,while the absorption maximum located at around 800 nm ensures deeper tissue penetration. However, its aqueous solutions are unstable due to its tendency to aggregate. ICG also binds strongly to plasma proteins, which leads to

a decrease in systemic circulation time [17–25]. These shortcomings can be circumvented by utilizing nanoparticle drug delivery systems to encapsulate and protect ICG molecules. Several different nanoparticle platforms incorporating ICG have been studied so far, however these formulations either utilize ICG only as a fluorescent marker or in combination with a chemotherapeutic agent. Anticancer effects of ICG alone, encapsulated in a drug delivery system, still need to be studied.

1.2 Objectives

1. To encapsulate ICG in PLA nanospheres exhibiting high drug loading with suitable diameter, by nanoprecipitation
2. To characterize ICGNP in terms of size, zeta potential and drug loading capacity as well as photothermal and photodynamic capabilities
3. To employ ICGNP on cancer cells to assess their phototherapeutic activity

1.3 Outline

Chapter One presents the motivation and aims of the study.

Chapter Two contains the theoretical background on phototherapy and polymeric nanoparticle drug delivery systems. This chapter also aims to describe the properties of indocyanine green as well as the methods of production for the polymeric nanoparticles used in the study.

Chapter Three details the study on the ICG loaded PLA nanoparticle characteristics and the determination of optimal parameters for their production as well as the characterization of final nanoparticle formulation.

Chapter Four is concerned about the phototherapeutic effects of these nanopar-

ticles on prostate cancer cells, in vitro.

Chapter Five provides a final remarks on the results obtained and predictions about future directions.

2. BACKGROUND

2.1 Anticancer Phototherapy

Anticancer phototherapy involves the use of light irradiation combined with a photoactive agent (photosensitizer or photothermal agent) to destroy cancer cells. This treatment modality offers some advantages over conventional treatments such as; being minimally invasive and having minimal damage on healthy cells. The affected area can be precisely controlled by changing the spot size, irradiation, and power of the light source, providing control over the destructive effect of the treatment [26, 27]. The photoactive agents utilized in phototherapy localize in tumor cells and are known to be non-toxic in the absence of light, further limiting the affected area to include mainly cancerous cells. Due to this precise control on affected tissues phototherapy sessions can be repeated as necessary without inciting deleterious effects.

Two types of phototherapy, namely, photothermal therapy (PTT) and photodynamic therapy (PDT) are extensively studied. Both of these treatments require the administration of external agents to trap photons which are, in turn, transformed into heat or reactive oxygen species (ROS). The essential components for both types of therapy are photoactive agents, and light at appropriate wavelength to activate these agents.

Although photoactive agents can also be stimulated with broadband light, such as sunlight, advancement in phototherapy gained momentum after the invention of the laser. Light produced by a laser is monochromatic, which enables specific activation of molecules, and can easily be coupled to optical fibers, which facilitates delivery and control on irradiation volume. Furthermore, precise control on irradiation time and method (continuous or pulsed wave) allows for better regulated photothermal mechanism. The wavelength of light utilized in phototherapy generally ranges between 600-800 nm, where the optical window for biological tissues is placed. Photons of

this range are energetic enough to excite the photosensitizer, and also have sufficient penetration into tissue due to low absorption coefficients of indigenous chromophores in that interval [28] (Figure 2.1). Although light penetration into tissue continues to increase as far as 1600 nm, energy of photons decrease.Molecular oxygen requires at least 95 kJ/mol for sensitized singlet oxygen to form, which should be the least amount of energy the triplet state of the PS molecule to have (assuming transfer without loss). Since triplet state of the PS molecule would form via intersystem crossing from excited singlet state PS and some of the energy would be lost during this process, even higher energy of singlet state PS would be required. This excited state is known to be the result of electronic excitation of ground level PS, which can only occur with the absorption of a photon of suitable energy. Therefore, there exist a limit on the irradiation wavelength to induce a photodynamic effect, further restraining the available irradiation wavelengths [29].

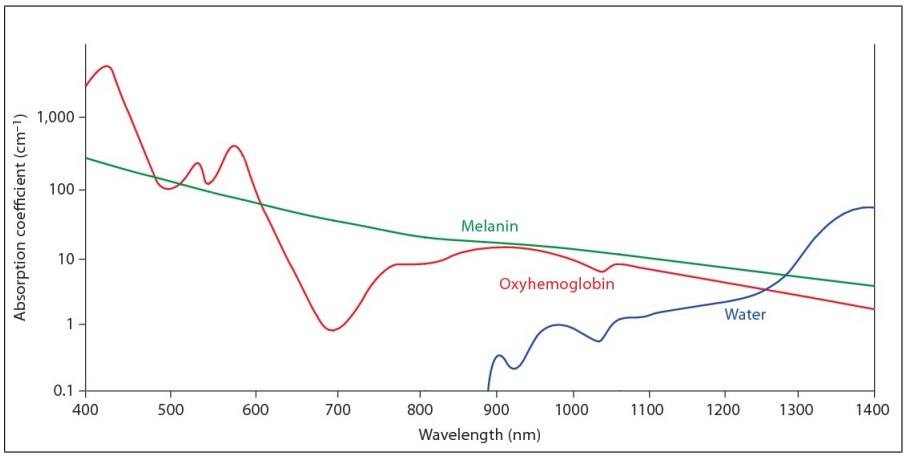

Figure 2.1 Most prominent indigenous chromophores of tissue. The optical therapeutic window lies in between 600 and 800 nm where the absorption by oxyhemoglobin is at its lowest. Although infrared ranges appear to be most suitable for light penetration in tissue due to decreasing trend in the absorption of melanin and hemoglobin, water becomes the major absorber after 1000 nm and NIR photons lack necessary energy to excite ground level oxygen molecules [30].

2.1.1 Photodynamic Therapy (PDT)

Three components are critical for the photodynamic effect to take place: photosensitizer molecule (PS), light at a specific wavelength and molecular oxygen. The interaction between these components produces ROS, which in turn results in the se-

lective destruction of target tissue by promoting oxidative stress. The PDT treatment begins with the administration of PS drug, which accumulates in the target tissue. Afterwards, exposure to the appropriate wavelength of light triggers the production of cytotoxic ROS in the target cells.

PS molecules themselves do not react with biomolecules, rather they transfer the energy of light to molecular oxygen or other substrates [27]. Electronic excitation of the PS molecule from ground state (S_0) to a singlet excited state (S_n) occurs upon absorption of a photon of sufficient energy. The excited state S_n relaxes to yield the lowest excited singlet state S_1. The excited molecule in S_1 can then either undergo intersystem crossing to a longer-lived and more reactive triplet state (T_1) or can relax back to ground state by light emission (fluorescence) or heat production. Excited triplet-state photosensitizer can then react in two different ways to initiate a photodynamic response. First one, Type I reaction, involves direct electron transfer from PS molecule to cellular substrates which generates free radicals. Since triplet-state PS has short lifetime, Type I reactions occur only if PS is in close vicinity of a suitable substrate. Second one, Type II reaction, involves energy transfer from energetic triplet state PS molecule to ground state molecular oxygen in a spin-allowed transition since excited PS and ground state oxygen are both in triplet states, producing highly reactive singlet oxygen ($^1O_2$) [31–33]. Since the amount of singlet oxygen produced is directly proportional to the number of triplet state PS molecules present, both the lifetime and triplet yield of PS are important properties in determination of their photosensitizing ability.

Jablonski diagram in Figure 2.2 summarize these pathways.

In order for effective ROS production to take place, a PS molecule should possess several characteristics. These are;

1. High absorption coefficient at irradiation wavelength
2. Good photostability

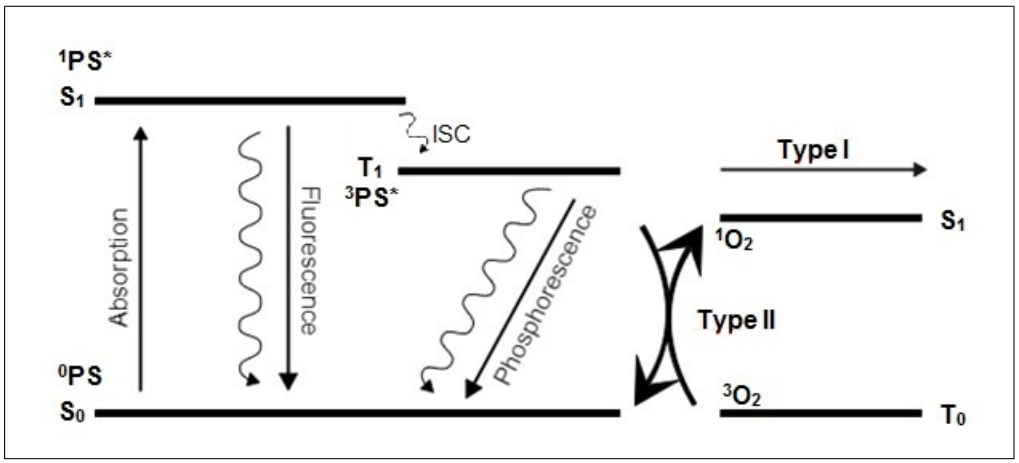

Figure 2.2 Jablonski diagram depicting PDT pathways. Absorption of a photon of suitable wavelength causes PS molecule to become excited (S_1), which then loses its excess energy either via fluorescence or intersystem crossing (ISC) to triplet state (T_1). Triplet state PS can then either interact with suitable substrates via redox reactions (Type I reaction), resulting in various ROS, or interact directly with ground level triplet oxygen (Type II reaction), resulting in singlet oxygen ($^1O_2$) production.

3. High quantum yield of triplet state with long triplet state lifetime and appropriate energy [32, 34]

Although the effect of other ROS species in PDT is incontrovertible, singlet oxygen is the primary cytotoxic product, responsible for the majority of the PDT effect. Therefore, singlet oxygen quantum yield (the amount of singlet oxygen molecules produced upon absorption of a single photon) is one of the most important properties of a PS molecule [35].

The lifetime of singlet oxygen in the cellular environment is measured to be around 3 μs [36]. Coupled with high reactivity, this short lifetime limits the diffusion of singlet oxygen, confining its effect to only targeted cells. However, since the reaction is highly dependent on the presence of molecular oxygen, the effectiveness of PDT in hypoxic tumors are, unfortunately, limited.

2.1.2 Photothermal Therapy (PTT)

The mechanism of photothermal therapy is similar to PDT, in the sense that it starts with the absorption of light. The absorbing molecules in this modality are called photothermal agents (PTA)(or photothermal tranduscers) capable of converting light photons into thermal energy through vibrational relaxation of higher energy states [35]. The use of PTA enables the treatment of difficult-to-treat tumors with minimal invasiveness and facilitates the treatment of advanced cancers via immunological stimulation [37].

These agents include dye molecules such as indocyanine green and nanomaterials based on noble metals or carbon. During local hyperthermia (heating to 41-47°C), heat produced in target cells causes irreversible damage in 30-60 min, while at slightly higher temperatures of 52°C 4 to 6 min is sufficient. As the local temperature exceeds 60 °C, the time required to attain irreversible cell damage exponentially decreases due to rather rapid protein denaturation and cell membrane disruption. Typically, photothermal damage commences at 41°C however, much higher temperatures in the tumor core are desired so that when the temperature gradient forms, cells on the outer edges of the tumor will also reach therapeutic temperatures [37].

PTT induced hyperthermia is more advantageous compared to conventional outside-in hyperthermia in which heating is achieved from outside, causing a temperature gradient on healthy tissue as well. In contrast, PTT achieves strictly localized hyperthermia, originating from the target cells and dissipating out and therefore, limiting damage to healthy tissues [4, 38].

Compared to PDT, limitations on PTT treatments are fewer since the reaction is independent of molecular oxygen levels. However, non-specific systemic distribution of PTA molecules still poses a problem. In order to overcome potential damage to healthy tissue, nanomaterial PTAs are developed that can selectively accumulate in target cells [39, 40].

2.2 Indocyanine Green (ICG)

Indocyanine green is an organic dye with amphiphilic nature, and is made up of two polycyclic units (benzoindotricarbocyanin) joined by a carbon chain as seen in Figure 2.3. These polycyclic moieties impart lipophilic properties to ICG, whereas sulfate groups provide hydrophilic characteristics. Consequently, ICG molecules are soluble in solvents such as DMSO as well as aqueous media [17]. In medicine, the use of ICG for diagnostic purposes (such as monitoring of hepatic or cardiac function or for ophthalmic angiography) is approved by the Food and Drug Administration (FDA). Moreover, ICG also acts as a photosensitizer and chromophore, resulting in numerous studies that investigate its potential as a phototherapy agent [7–16].

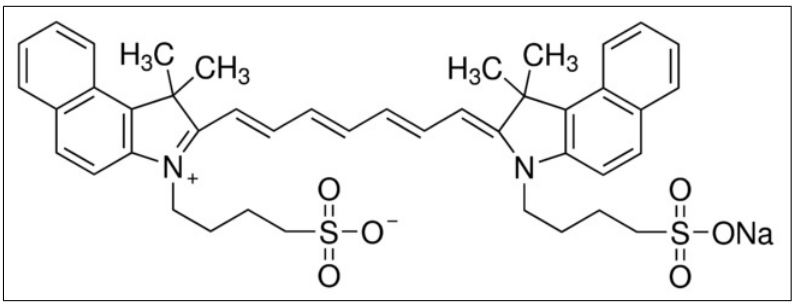

Figure 2.3 Chemical structure of indocyanine green [41].

As a phototherapy agent, the absorption spectrum of ICG was extensively studied. The major absorption peak of ICG is located around 800 nm however, the characteristics of the absorption spectrum depends heavily on the nature of the solvent and dye concentration. In aqueous solution, the absorption maximum of ICG is located at 775 nm for its monomeric form (at concentrations below 10 μM). Increasing dye concentration causes dimer and oligomer formation in the form of J-aggregation, evident as new peaks in spectrum forming around 700 nm as seen in Figure 2.4. Apparently, absorption coefficient of ICG is directly dependent on the concentration of dye, which means ICG generally does not follow Beer-Lambert's Law. However, at sufficiently low concentrations (below 12.5 μM) there exists a linear relation between optical density and concentration [20, 21, 25].

Upon intravenous administration, ICG is known to bind to plasma proteins,

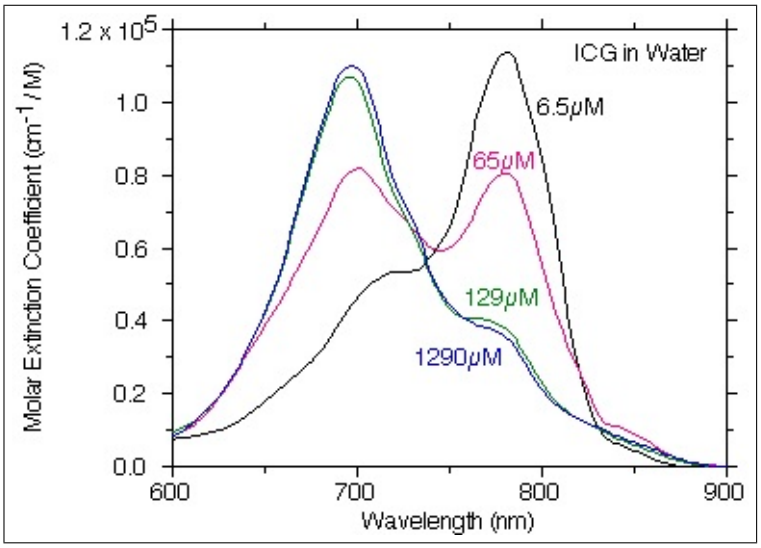

Figure 2.4 Absorption coefficient of ICG at various concentrations in water. In its monomeric form (at 6.5 μM) ICG absorption peak lies at 775 nm. Aggregation in dimer and oligomer forms are observed as new peak formation at around 700 nm. As concentration increases, corresponding aggregate peak at 700 nm also increases in optical density [42].

especially albumin by dye adsorption to macromolecular albumin nanoparticles. This phenomenon changes the absorption spectrum further, causing a bathochromic shift of the major peak to 805 nm as observed in Figure 2.5. Higher concentrations in plasma also induce aggregation due to amphiphilic nature of ICG, observed as new peaks at shorter wavelengths; however dye adsorption to albumin dominates over oligomerization [20, 25]. The non-specific binding tendency of ICG causes its pharmacokinetics to be extraordinarily fast. ICG promptly clears from the circulation with a half life of 3-4 min [43].

ICG is also found to be susceptible to heat-induced and light-induced degradation. Photoexcitation or thermal agitation of ICG solutions causes degradation of dye molecules, causing a decrease in absorption spectrum, although solutions containing serum or supplemented with albumin exhibit higher thermal and photostability. However, for J-aggregates or protein-bound ICG, thermal agitation or photoexcitation cannot cause conformational changes. This effect causes a prominent decrease of photosensitizing ability however; the increased thermal stability becomes advantageous for photothermal applications [19, 22–24].

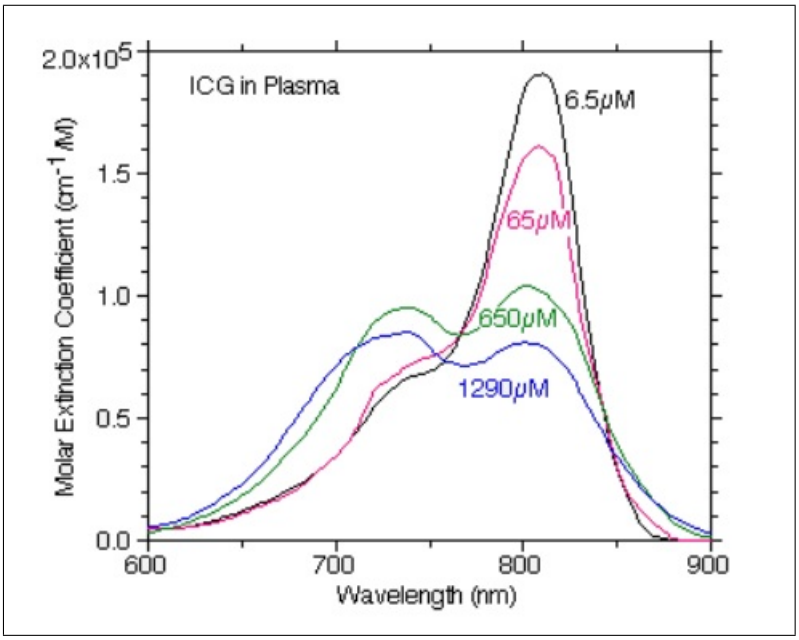

Figure 2.5 Absorption coefficient of ICG at various concentrations in plasma. Binding of ICG molecules to serum albumin causes a redshift (to 805 nm) in absorption peak. Aggregation due to increasing concentration can also be observed in plasma, although aggregate peak (also slightly redshifted to 720 nm) does not increase dramatically in optical density with increasing concentration [42].

Properties of ICG can be examined in the light of three characteristics of an ideal PS. First of these characteristics is to have high absorption coefficient at irradiation wavelength. Absorption coefficient can be calculated using molar extinction coefficients using Eq. 2.1.

$$\mu_a = 2.303 \times e \times C \tag{2.1}$$

where μ_a is absorption coefficient, e is molar extinction coefficient and C is concentration of dye.Unfortunately, molar extinction coefficients for ICG vary with concentration, due to aggregation of molecules at higher concentrations. The decrease in molar extinction coefficient of ICG with increasing concentration can be observed in Table 2.1.

Even though molar extinction coefficient of ICG decreases with increasing concentration, absorption coefficients increase sufficiently.(For comparative purposes, molar extinction coefficient of methylene blue is 4.3×10^4 at 632 nm [44].)

Table 2.1
Molar extinction coefficient and absorption coefficient of ICG at different concentrations (data used in calculations from Landsman et al. [21]).

$C\ (\mu M)$	e @ 808 nm (cm^{-1}/M)	$\mu_a\ (cm^{-1})$
6.5	6×10^4	90×10^{-2}
65	4×10^4	598×10^{-2}
650	1.7×10^4	2542×10^{-2}

Second characteristic to consider in a good photosensitizer is good photostability. ICG in monomeric form is reported to be rather unstable in water, whereas J-aggregates are more stable. Moreover, changing solvent to methanol or DMSO significantly increases the photostability. ICG bound to proteins in human plasma is also reported to be quite stable, since strong conformational changes due to electronic excitation becomes harder, reducing radical forming bond-braking [22]. Furthermore, photodegredation of ICG is observed to be wavelength-dependent, with a faster decay at 808 nm than 780 nm irradiation [45].

Triplet state quantum yield is another important factor to evaluate for a PS molecule. For ICG in water, triplet formation quantum yield is estimated to be $\Phi_{ST}(H_2O) = 2.2 \pm 0.7 \times 10^{-3}$ with yield of 14% and effective triplet lifetime of approximately $10^{-9} - 10^{-4}$ s, providing sufficient time for dye radical reaction with solvent radicals [22, 45, 46].The reported triplet yield is deemed sufficient for singlet oxygen generation [46].

As a photothermal therapy agent, ICG is demonstrated to induce concentration dependent temperature elevation. Temperature of aqueous solutions of ICG rise rapidly under irradiation of a suitable wavelength even at low concentrations ($\Delta T_{max} = 5$°C at 6 μM; $\Delta T_{max} = 28.5$°C at 24 μM). *In vivo* temperature elevation in tumor models is significantly affected by ICG concentration, but the contribution of laser power density to temperature elevation is less pronounced [47].

Although ICG does not exhibit good photostability and quite low quantum

yield of triplet state, it makes up for these drawbacks with its long-lived triplet state and good absorption coefficient in the near-infrared region. However, its tendency to aggregate and bind to plasma proteins reduces the photodynamic efficiency. In order to improve the efficiency of ICG-PDT, encapsulation of dye in nanoparticle drug delivery systems is proposed.

2.3 Nanoparticle Drug Delivery Systems (Nano DDS)

Drug delivery is a method to control the in vivo distribution of drug molecules by utilizing chemical and biological principles. Upon administration, only a small fraction of drug molecules normally reach its intended destination, most of the dose either gets cleared from circulation or ends up in irrelevant tissues. This is especially problematic with chemotherapeutics, which are known to be cytostatic or cytotoxic therefore their uptake by healthy cells pose a threat [48]. As a result, implementing a nanomedicine approach where nano-sized carriers are used to deliver these drug molecules was proposed. These drug loaded nanocarriers are advantageous for anticancer therapies since they are capable of keeping the drug in circulation for extended periods of time and can increase the uptake by tumors. This is either achieved through active targeting of nanoparticles to tumor cells via surface decoration, or passive targeting due to enhanced permeability and retention (EPR) effect [6]. EPR effect is a direct result of faulty angiogenesis in tumors, causing hypervascularization with a defective endothelial cell layer, and a lack of lymphatic drainage. The vasculature with discontinuous endothelium defined by large fenestration can allow entry for particles as large as 780 nm [49]. Nanoparticles avoid renal clearance due to their large size and cannot penetrate the tight endothelial junctions of normal blood vessels, which increases their circulation time. Since tumor vasculature has wider gaps between endothelial linings; most of the nanoparticles accumulate in tumor cells and are stuck inside as a result of the lack of lymphatic drainage [50].

Several different nanocarrier systems are investigated for drug delivery applications, ranging from polymeric nanoparticles to dendrimers and inorganic nanoparticles.

Amongst these, polymeric nanoparticles are of particular concern, due to their good biocompatibility, ease of production, relatively low cost and ease of surface modifications for tailored purposes. Therefore, polymeric nanoparticles are excellent platforms on which conventional treatments of cancer (chemotherapy) can meet with other treatments such as phototherapy for increased efficiency in cancer treatment [26, 39].

Polymeric nanoparticles are solid, colloidal particles with dimensions in the range of 100 to 500 nm and are synthesized from biodegradable or biocompatible materials. These polymeric materials can either be natural; such as chitosan, alginate or collagen, or synthetic such as poly (d, l-lactic acid) (PLA), poly (d, l-lactic-co-glycolic acid) (PLGA) and poly (e-caprolactone) (PCL) [5,51]. Amongst these, PLA and PLGA are the most studied for drug delivery applications due to their biocompatibility and low toxicity. Furthermore, they have the US Food and Drug Administration (FDA) approval for a variety of biomedical applications, including drug delivery applications. PLA and PLGA micro/nanospheres containing bioactive agents are repeatedly documented to be biocompatible and their in vivo applications do not prompt local or systemic adverse results. Biodegradation of PLA nanoparticles takes place through hydrolytic chain cleavage with the polymer degradation rates on the surface and the bulk of the nanoparticles are similar [52].

In biological environments, PLA hydrolyzes into soluble oligomers which are then metabolized by cells. Aside from its biodegradability, PLA is also cost-effective since it is synthesized from agriculture-based products, making it a favorable candidate for drug delivery applications [53, 54].

PLA nanoparticles can be produced via different methods such as; emulsion/solvent evaporation, nanoprecipitation or salting-out. Among these methods, nanoprecipitation is widely used due to its fast and simple nature. Nanoparticles with a diameter of 50 to 300 nm with low polydspersity can easily be produced with this technique. Moreover, the setup used is relatively easy and cheap compared to other methods. Yield of the nanoparticles obtained via nanoprecipitation is high and toxic solvent use can be kept to a minimum [51, 55].

Three basic components make up the nanoprecipitation system: the polymer, solvent (in which the polymer is soluble) and the non-solvent (in which the polymer is insoluble). The solvent phase has to be miscible with the non-solvent phase. For most of the systems tested in the literature, non-solvent phase is water. The non-solvent phase, on the other hand, can be any polymer solvent that is miscible with water, and is mostly chosen as acetone, ethanol or methanol due to the ease of removal by evaporation [56–58].

The solvent phase, containing the polymer at low concentrations (<2%) is added dropwise to large amounts of non-solvent phase (which may or may not contain surfactants as a stabilizer). As the solvent phase is completely miscible in non-solvent phase, the excess amount of non-solvent in the mixture causes the polymer to become insoluble, inducing phase separation. The two conditions or miscibility and solubility must be met in order for nanoparticles to be formed. Although this method is most suitable to encapsulate lipophilic drugs, which are added to the solvent phase, amphiphilic or hydrophilic drugs can also be loaded via the same procedure (albeit at lower loading efficiencies) [51, 57].

The characteristics of the nanoparticles produced depends on many parameters such as the nature of solvent phase, polymer concentration, polymer molecular weight, volume ratio of solvent and non-solvent phases, stirring rate and surfactant concentration. Therefore it is important to choose suitable components and operation conditions to obtain well defined nanoparticles. Among available solvents for PLA, acetone is widely used because it has been shown to produce the smallest nanoparticles. As for the polymer concentration, smaller nanoparticles are known to be produced with low PLA concentrations (5 to 10 mg/mL) whereas further increase in concentration induces a dramatic increase in particle diameter. Another important parameter to take into consideration is solvent/non-solvent volume ratio (S/NS). Lower ratios are shown to produce smaller nanoparticles, whereas increasing the ratio to 0.6 or higher is observed to yield much larger nanoparticles with considerable aggregation [59–62].

2.4 Indocyanine Green Loaded Polymeric Nanoparticles for Phototherapy of Cancer

Indocyanine green incorporation into polymeric nanoparticles was previously studied, utilizing polymers ranging from synthetic (PLGA or PCL) to natural (chitosan or albumin) [63]. However, systems incorporating only ICG are few and most nanoparticles proposed also contain a chemotherapeutic agent as well. Furthermore, due to its fluorescent properties, some nanoplatforms employ ICG only for imaging purposes, as a fluorescent marker. The studies in which the sole role of ICG is imaging are beyond the scope of this dissertation and will not be discussed.

Encapsulation of ICG in PLGA nanoparticles was studied by Saxena et al, in which PLGA nanoparticles loaded with ICG were produced in sizes ranging from 300 to 800 nm. The parameters affecting the nanoparticle characteristics were discussed and encapsulation in polymeric matrix was shown to increase the thermal and photostability of ICG [64, 65]. These ICG-PLGA nanoparticles were used on P388-D1 cells to demonstrate their phototoxicity, by Gomes et al, who deemed these nanoparticles useful for photomedicine [66]. ICG-PLGA nanoparticles were recently used on PC3 cells by Patel et al, to demonstrate their non-toxicity in the dark. Furthermore, upon irradiation in a tissue phantom, ICG-PLGA nanoparticles were shown to provide good photothermal conversion properties [67]. Phototherapeutic effect of Anti-HER2 targeted ICG-PLGA-PEG nanoparticles on breast cancer cells were investigated by Lee et al., who reported more than 90% cell eradication at 25 μM ICG equivalent upon irradiation (6 W/cm^2, 5 min) [68]. Zhao et al studied ICG loaded PLGA-lecithin-PEG nanoparticles of three different sizes (39, 68 and 116 nm). These nanoparticles exhibited improved ICG stability and enhanced temperature response compared to free ICG. Employed on pancreatic carcinoma model, nanoparticles 68 nm in size achieved complete tumor suppression after irradiation with 808 nm laser (800 mW/cm^2, 10 min). Although the smallest type of nanoparticles exhibited better phototherapeutic response *in vitro*, retention of 68 nm in tumor was observed to be better *in vivo*, leading to better tumor volume suppression [69].

In another study, chitosan was used to enhance the loading of ICG in PLGA nanoparticles, along with carboplatin. This approach yielded PLGA nanoparticles with better ICG loading capacity at a diameter of 200 nm. Upon irradiation (808 nm, 2W for 10 min, 1528 J/cm^2) these nanoparticles provided complete cell growth inhibition on SKOV3 cells [70].

Despite the fact that these studies reported promising results for phototherapy with ICG loaded nanoparticles, most systems opted to incorporate a chemotherapy agent alongside ICG to obtain better cell suppression. Most chemotherapy drugs exhibit inadequate aqueous solubility, which hinders their administration but can be circumvented by utilizing a drug delivery system. Moreover, the thermal effect of phototherapy was observed to increase the effectiveness of chemotherapy, therefore many drug delivery systems intended for phototherapy also contain a chemotherapy agent as well.

Several examples exist in the literature for nanoparticles containing ICG alongside a chemotherapy agent, the most popular being doxorubicin (DOX). PLGA nanoparticles encapsulating ICG and DOX were investigated for combinatorial chemo/ phototherapy [71–73]. Other polymers were also tested to deliver the same combination, such as poly (glutamic acid)-g-PLGA functionalized with cholesterol-PEG (chen) which exhibited good PTT effect under irradiation (808 nm, 0.75 W/cm^2, 6 min). A targeted nanoparticle system produced via self-assembly of lecithin and PCL and loaded with ICG and DOX was also studied. On MDA-MB-231 and A549 cells, these nanoparticles resulted in more than 90% cell death upon irradiation (1W/cm^2, 5 min) with good photothermal and photodynamic effects [74]. Lin et al examined PLGA nanoparticles designed with an immunotherapy agent, resiquimod and managed to obtain almost complete cell eradication even at low doses of ICG (80 μM ICG, 808 nm, 1W/cm^2, 10 min) [75].

Combinations of other polymers with various chemotherapeutic agents along with ICG were examined as well, such as bovine serum albumin (BSA) nanoparticles loaded with ICG and DOX, which exhibit good ROS production coupled with good

photothermal conversion capability. Irradiation (1 W/cm^2, 4 min) of MCF-7 cells incubated with these nanoparticles yielded around 80% cell death [76]. On the other hand, albumin nanoparticles loaded with ICG and paclitaxel (PTX) were investigated by Kim et al. Tested on pancreatic cancer cells, these nanoparticles eradicated 80% of the cells upon irradiation (1.5W/cm^2, 10 min) [77].

Curcumin is another anticancer agent that was co-loaded with ICG in albumin nanoparticles. These nanoparticles were observed to be effective in producing mild hyperthermia (1.5W/cm^2, 5 min), which synergistically increases the anticancer effect of curcumin [78].

It is evident that ICG is incorporated in various different types of nanoparticles to be used as an anticancer agent continues to be a topic of interest. However, the phototherapeutic effects of only ICG containing polymeric nanoparticles need to be studied further for a better understanding of the role ICG plays.

3. ICG LOADED PLA NANOPARTICLES: PREPARATION AND CHARACTERIZATION

3.1 Introduction

Most of the studies involving encapsulation of ICG in a polymeric nanoparticle system utilized PLGA as carrier polymer. These nanoparticles were investigated in terms of the parameters which affected nanoparticle characteristics [64, 66], as well as in terms of their effects on various cell lines [66–68]. Table 3.1 and Table 3.2 summarizes the methods utilized in these studies along with the results obtained.

Table 3.1
Studies on ICG-encapsulating PLGA nanoparticles produced via emulsification/solvent evaporation technique (asterisk denotes studies with more than one formulation).

Method: Emulsion/solvent evaporation					
Formulation	Size	ζ Potential	%EE	%LC	Reference
(62.5 mg/mL PLGA in DCM; 50 μM ICG) emulsified in 3% PVA	817±70 nm	N/A	65%	N/A	[66]
(30mg/mL PLGA in DCM; 1 mM ICG) emulsified in 5% PVA	246±11 nm	-18 mV	48.8%	0.57%	[67]
(50 mg/mL PLGA in DCM; 2.6 mM ICG; 37 mM DOX) emulsified in 3% PVA containing 2 mg ICG; 4 mg BSA	235 nm	-20 mV	32.8% (DOX); 71.6% (ICG)	N/A	[79]
(15 mg/mL PLGA in methanol+DCM; 330 μM ICG; 460 μM DOX) emulsified in 3% PVA	167±5 nm	-11.3 mV	45% (ICG); 70% (DOX)	1.8% (ICG); 2.3% (DOX)	[71]
(15 mg/mL PLGA in methanol+DCM; 330 μM ICG; 460 μM DOX) emulsified in 3% PVA	135±1.4 nm	-11.8 mV	N/A	3% (ICG); 4% (DOX)	[72]
(13-66 mg/mL PLGA; 15-35 μM ICG; 17-37 μM DOX in methanol+DCM) emulsified in 1-5% PVA	137-164 nm	-10, -12 mV	44% (ICG); 74% (DOX)	0.015% (ICG); 0.022% (DOX)	[73] *
(30 mg/mL PLGA; 1.3 mM ICG in methanol+DCM) emulsified in 0.2% PVA	307±4.6 nm	-17.3 mV	75%	2.6%	[68]

Table 3.2
Studies on ICG-encapsulating PLGA and PLA nanoparticles produced via nanoprecipitation (asterisk denotes studies with more than one formulation).

Method: Nanoprecipitation					
Formulation	Size	ζ Potential	%EE	%LC	Reference
(4-33 mg/mL PLGA in acetonitrile; 53-530 μM ICG in methanol) added to 4% aqueous PVA (S/NS: 1/5)	350-405 nm	N/A	N/A	0.30% max	[64] *
(33 mg/mL PLGA in acetonitrile; 53μM ICG in methanol) added to 4% aqueous PVA (S/NS: 1/5)	357±2 nm	N/A	74.5%	0.20%	[80]
(15 mg/mL PLA-mPEG; 1.3 mM ICG; 2.9 mM DOX in acetone+DMSO) added to ultrapure water (S/NS:1/20)	108±2 nm	-7.7±1.2 mV	N/A	4.2% (DOX); 2.1% (ICG)	[81]
(10 mg/mL PLGA; 1.9 mM DTX; 323μM ICG; 0.5 mg/mL DSPE-PEG2000; 0.5 mg/mL DSPE-PEG2000-Mal in acetone+methanol) added to aqueous BSA (S/NS:1/4)	221±1.6 nm	-22.2mV	42% (ICG); 93% (DTX)	N/A	[82]

As demonstrated in these studies, ICG could be successfully encapsulated in polymeric matrix, although loading capacities varied considerably among formulations. In general, emulsification/solvent evaporation technique tended to produce nanoparticles with higher drug loading capacity than nanoprecipitation.

Effects of different parameters on nanoparticle characteristics were investigated in only two of these studies [64, 73]. Manchanda et al. examined the effects of polymer concentration, ICG and DOX concentrations, and PVA concentration on particle size, zeta potential and encapsulation efficiency, employing a single emulsion/solvent evaporation technique. According to the results obtained in this study, increasing PLGA concentrations caused increased nanoparticle size due to increased viscosity, which in turn yields larger droplets upon emulsification. Increased PLGA amount also increased encapsulation efficiency up to a point, possibly due to the increase in particle size. Drug concentration (for both ICG and DOX) were found to be ineffective on particle size. On the other hand, increasing PVA concentration was found to yield significantly smaller nanoparticles with decreasing entrapment efficiency. The optimal formulation for this study was reported as 53 mg/mL PLGA, 20 μM ICG and 22 μM DOX emulsified in 1% aqueous PVA solution. This formulation yielded nanoparticles 171 nm in diameter with 0.015% ICG and 0.022% DOX loading [73].

Moreover, Saxena et al. studied the effects of PLGA amount and ICG amount in the formulation on nanoparticle characteristics, produced via nanoprecipitation. This study utilized a fixed S/NS ratio of 1/5 while employing two different polymer amounts (4 mg/mL and 33 mg/mL) along with three different ICG amounts (1, 5 or 10 mg ICG corresponding to 53, 269 and 530 μM). The study reported no significant difference on particle size with different polymer amounts although sizes of different formulations ranged from 307 to 405 nm. Furthermore, ICG amount was also reported to have no effect on particle size. On the other hand, increased polymer amount caused an increase in encapsulation efficiency, which was explained by increased availability of polymer in formulation to entrap ICG molecules. In terms of loading capacity, increasing ICG concentration from 53 to 269 μM boosted the loading capacity, whereas further increase to 530 μM caused a decline [64].

Some of these studies examine the photothermal and photodynamic capabilities of these nanoparticles as well. Patel et al. reported better photothermal conversion capability of PLGA-ICG nanoparticles compared to free ICG, causing a $\Delta T_{max} \cong 10$ °C upon irradiation with 808 nm laser at 240 J/cm^2 when utilized in a tissue phantom [67]. Same type of nanoparticles were reported to exhibit heating capabilities comparable to free ICG at all concentrations tested ($\Delta T_{max} \cong 45$ °C for 25 μM,1800 J/cm^2) [68]. Moreover, ICG-DOX-PLGA were reported to be capable of inducing mild hyperthermia ($T_{max} = 43°C$) at $5\mu M$) when irradiated at 1440 J/cm^2, which was demonstrated to increase the cytotoxicity of DOX([71, 72]. On the other hand, ICG-DTX-PLGA nanoparticles at 12 μM ICg-equivalent concentration were observed to heat up to 53°C when irradiated at 750 J/cm^2 (compared to $T_{max} = 56°C$ obtained with free ICG) [82].

Singlet oxygen production of encapsulated ICG was demonstrated in one study, in which a fluorescent probe was used to monitor the amount of singlet oxygen produced upon irradiation. Both free ICG and ICG-PLGA exhibited same amount of singlet oxygen production up to 25 μM [68]. Intracellular ROS increase due to ICG-DTX-PLGA uptake were also evaluated at 12 μM concentration and was reported to be significantly higher than free ICG induced ROS production under same circumstances [82].

In this study, results of these previous research were adapted to be used for PLA nanoparticles. Effects of several parameters on nanoparticle characteristics were investigated in order to obtain nanoparticles with higher drug loading capacity and suitable size. Photothermal conversion and ROS production capabilities of these nanoparticles were also investigated along with their size, morphology, drug loading capacity and yield.

The aim of this study is to investigate the parameters affecting nanoparticle characteristics, to determine the formulation that produces nanoparticles with optimal properties and to characterize said nanoparticles.

3.2 Materials and Methods

3.2.1 Preparation of nanoparticles

All chemicals were purchased from Sigma-Aldrich (Darmstadt, Germany). Nanoprecipitation method was used to prepare nanoparticles for all experiments. For this procedure 10 mg/mL PLA (average Mn 20000) was dissolved in acetone (99.8%) and injected in ultrapure water containing ICG (I2633) and 2% PVA (MW 13000 - 23000, 87 - 89% hydrolyzed) under magnetic stirring (500 rpm) as seen in Figure 3.1. Nanoparticles (ICGNP) were instantly formed upon injection. The suspension was stirred for 10 min, centrifuged at 1500g for 15 min to remove the aggregates and the supernatants were centrifuged again at 10.000g 15 min to obtain the nanoparticles. The pellets were washed thrice with ultrapure water and lyophilized for 48 h (Christ, Alpha 2–4LD plus, Germany). Dry nanoparticles were kept in bottles shrouded with foil at 4 °C.

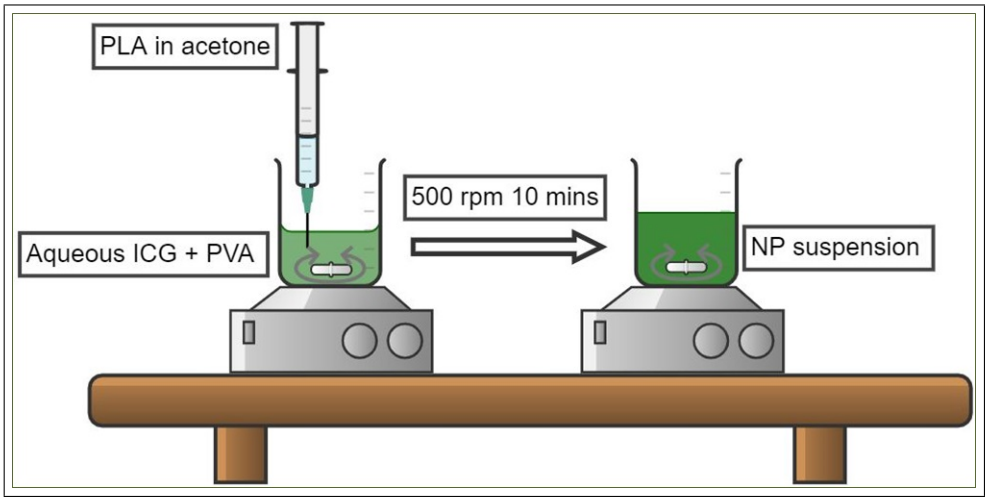

Figure 3.1 Schematic of nanoprecipitation setup used to prepare the ICGNP. PLA dissolved in acetone was slowly injected into ICG containing aqueous PVA as a stabilizer. Nanoparticles were aged for 10 min under mild magnetic stirring and then collected via centrifugation.

Various levels of solvent/non-solvent ratio (S/NS) and ICG concentration were investigated in a one-factor-at-a-time fashion, to ascertain their effects on nanoparticle characteristics such as size and loading capacity. The levels for parameters are summarized in Table 3.3. For S/NS ratio, ICG concentration was kept at 50 μM and non-solvent volume was kept at 10 mL while solvent volume changed to adjust S/NS

to 1/2, 1/3, 1/10 and 1/20. For ICG concentration; S/NS ratio was kept at 1/3 while ICG concentration was adjusted in between 30 to 1000 μM.

Table 3.3
Parameters used to examine the effects of S/NS ratio and ICG concentration in nanoparticle characteristics.

Effect of S/NS ratio	
Solvent Phase (S)	10 mg/mL PLA in acetone
Non-Solvent Phase (NS)	50 μM ICG in 2% aqueous PVA
S/NS ratio	1/2, 1/3, 1/10, 1/20
Effect of ICG concentration	
Solvent Phase (S)	10 mg/mL PLA in acetone
Non-Solvent Phase (NS)	30, 50, 80, 110, 150, 200, 500, 1000 μM ICG in 2% aqueous PVA
S/NS ratio	1/3

3.2.2 Laser setup

Irradiation of samples was achieved via a custom-built computer-controlled laser diode operating in continuous wave (CW) mode at 809 nm output wavelength as shown in Figure 3.2. Output fiber was positioned to produce a homogeneous beam of diameter 1.9 cm, irradiation spot size 2.84 cm^2, sufficient to irradiate 4-well area of a 96 well plate at once. Laser power density was measured with the help of a optical powermeter (1918-R, Newport, CA, USA). Irradiance was kept at 1 W/cm^2 for all experiments, while fluence was adjusted by changing the irradiation time.

3.2.3 Characterization of nanoparticles

The size and zeta potential of nanoparticles were measured using dynamic light scattering (DLS; Brookhaven Instruments 90Plus Particle Size/ Zeta Analyzer, NY, USA). SEM and STEM images were taken to confirm the spherical morphology and structure of ICGNP from samples air dried at room temperature on copper grids (FEI-Philips XL30 ESEM FEG, utilizing STEM detector).

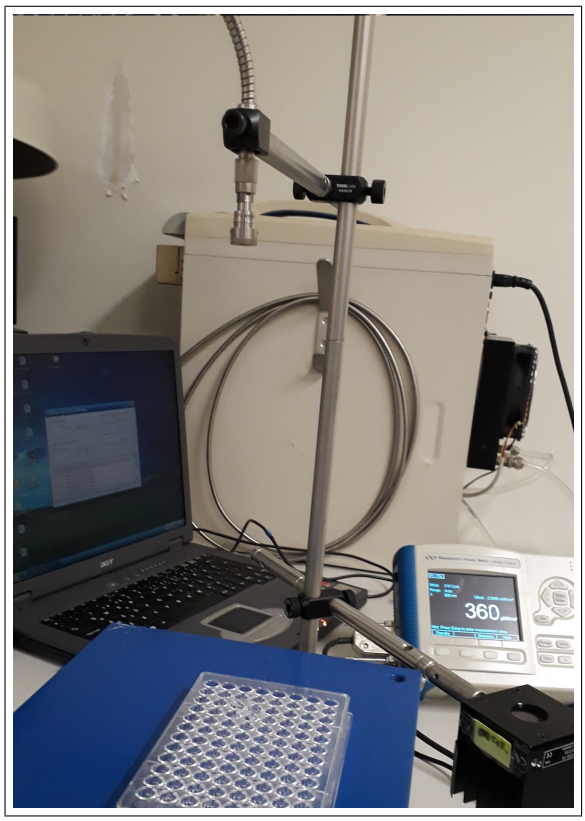

Figure 3.2 Computer controlled diode laser setup with height adjustable stage and powermeter.

Absorption spectra of ICG and ICGNP were recorded using a micro-volume spectrophotometer (NanoDrop 2000c, Thermo Scientific, MA, USA).Samples prepared in complete cell culture medium at concentrations 25, 50 and 100 μM of ICG were measured using 2 μL samples on pedestal. Obtained spectra were plotted and processed via Spectragryph software (Spectragryph optical spectroscopy software, Friedrich Menges PhD).

Nanoparticle yield was calculated via Eq. 3.1 after lyophilized nanoparticles were weighted.

$$Yield = (\frac{Experimental\ Mass}{Theoretical\ Mass}) \times 100 \tag{3.1}$$

ICG content of nanoparticles were determined spectrophotometrically. Standards of ICG in DMSO were prepared at the concentration range 1-7 μM where ICG is known to follow Lambert-Beer's Law. The absorbance values of the standards at 795 nm were used to construct a calibration curve as seen in Figure 3.3. Lyophilized nanoparticles obtained from different formulations were dissolved in DMSO and their absorbances at 795 nm were used to calculate the amount of ICG encapsulated. Encapsulation efficiency (%EE) and loading capacity (%LC) were calculated according to Eq. 3.2 and 3.3.

$$\%EE = \left(\frac{Amount\ of\ encapsulated\ drug}{Amount\ of\ total\ drug\ in\ formulation}\right) \times 100 \tag{3.2}$$

$$\%LC = \left(\frac{Mass\ of\ encapsulated\ drug}{Mass\ of\ total\ nanoparticles\ recovered}\right) \times 100 \tag{3.3}$$

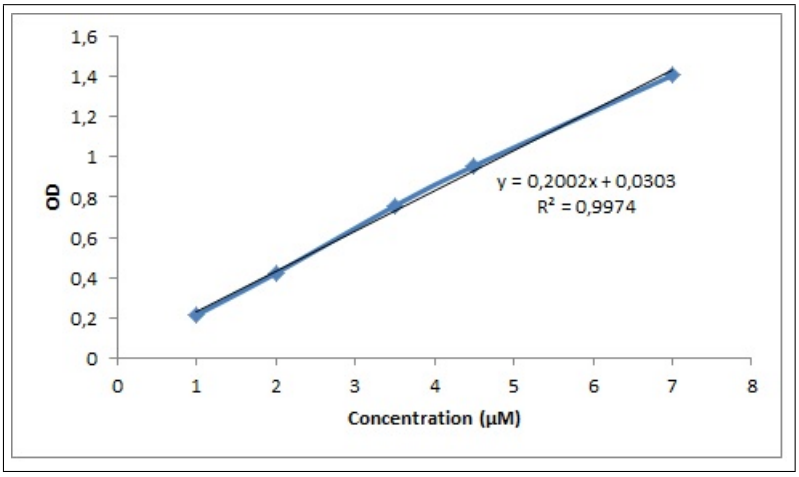

Figure 3.3 Calibration curve for ICG in DMSO. Absorbance measured at 795 nm, in spectrophotometry cuvette, pathlength=10 mm. n=3 for each data point.

Drug release from nanoparticles was also monitored spectrophotometrically. Another calibration curve of ICG was established in PBS using the same concentration range at 795 nm. 2 mL aliquots of ICGNP at the ICG-equivalent concentration of 25 μM were prepared in PBS at pH 7.4 and incubated at 37 °C. At regular intervals, the samples were centrifuged at 10.000g for 15 min, supernatant absorptions at 795

nm were measured and the pellets were immediately resuspended in fresh PBS. Measured absorption values were used to calculate the ICG concentration released from the nanoparticles.

ROS production capability of ICGNP were observed indirectly, utilizing 1,3-diphenylisobenzofuran DPBF, whose absorption at 410 nm decreases in the presence of singlet oxygen. ICG and ICGNP solutions at 10, 30 and 50 μM were prepared in a mixture of ethanol and distilled water (4:1; v:v) and supplemented with DPBF at a fixed concentration. The samples were then irradiated repeatedly for 15 s at 100 mW/cm^2, and absorption of DPBF at 410 nm was measured at the beginning and the end of every 15 s interval. The change in DPBF absorption with respect to irradiation time was plotted.

Photothermal conversion capability of ICGNP was observed with the help of a T-type thermocouple (MT-29/1, Physitemp, NJ, USA). Solutions containing ICG or ICGNP at concentrations 10, 30 and 50 μM were prepared in cell culture medium and irradiated in 4 mL spectrophotometry cuvettes at 1 W/cm^2. Thermocouple needle was inserted into the liquid and the temperature was read at 20 s intervals for 400 s.

3.2.4 Statistical analysis

All characterization experiments were conducted in triplicate. Reported data were formatted as mean ± standard deviation. Statistical analysis was performed using ANOVA followed by Tukey's test to determine whether any significant difference exists between groups at $p \leq 0.05$ level.

3.3 Results

Nanoparticles were formed upon solvent phase injection, which was observed as an increased turbidity of the mixture due to light scattering from particles. The

suspensions were centrifuged to separate the nanoparticles from unencapsulated drug. Aggregates were also observed to be formed alongside nanoparticle, which was evident in DLS measurements.Therefore suspensions were pre-centrifuged to remove the aggregates before size measurement and characterization.

3.3.1 Effects of S/NS ratio on nanoparticle characteristics

The effects of S/NS ratio on size, encapsulation efficiency, loading capacity and yield of nanoparticles produced were examined by keeping other two parameters constant at 10 mg/mL for PLA concentration and 50 μM for ICG concentration. The results, as shown in Table 3.4, indicate an increase in nanoparticle size with increasing S/NS ratio. However, no significant difference in terms of particle size were observed in between different formulations.

Table 3.4
Effects of S/NS ratio on nanoparticle characteristics.Each formulation contains 10 mg/mL PLA, 50 μM ICG, n=3.

S/NS ratio	Size (nm)	EE (%)	LC(%)	Yield (%)
1/20	245.9±35	0.67±0.2	0.08±0.03	62.5±3
1/10	270.2±20	1.79±6.6	0.11±0.01	48.3±12
1/3	289.2±24	5.15±1.4	0.14±0.01	42.3±12
1/2	300.4±10	3.13±1.1	0.06±0.02	38.3±7

Both encapsulation efficiency (%EE) and loading capacity (%LC) were observed to increase proportionally with S/NS ratio, up to 1/3, where maxima were reached. The results obtained at 1/3 ratio were significantly higher that the results of 1/20 group ($p \leq 0.05$). After this point, further increase in S/NS ratio to 1/2 caused a decline in the encapsulated drug, as seen in Figure 3.4. ICGNP produced at different S/NS ratio exhibited clearly distinguished %LC characteristics as observed in Figure 3.5.

The amount of recovered nanoparticles (yield) decreases, although not statistically significantly, with increasing S/NS ratio.

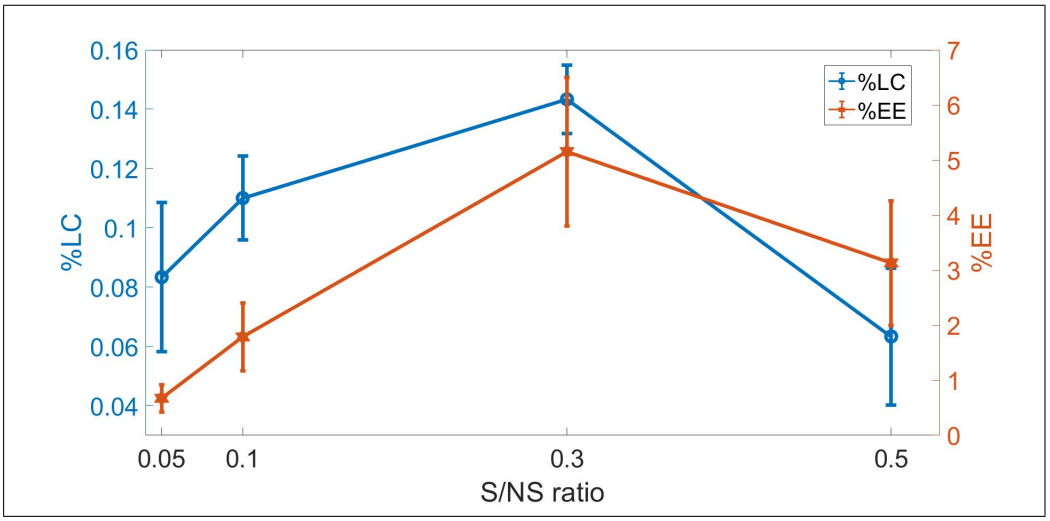

Figure 3.4 The effect of S/NS ratio on encapsulation efficiency (%EE) and loading capacity (%LC) of nanoparticles. Both %LC and %EE increase significantly as S/NS ratio increased from 0.05 to 0.3. However, further increase of S/NS ratio to 0.5 resulted in a sharp decline in both %LC and %EE, which is statistically significant.

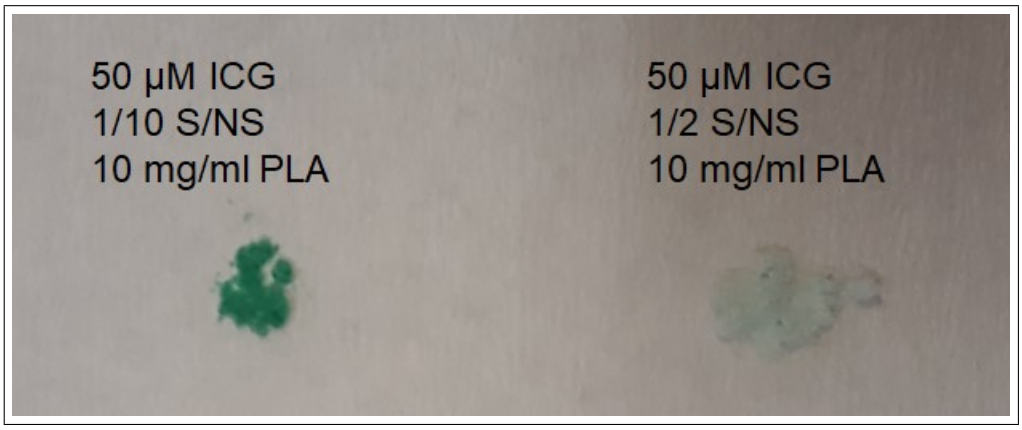

Figure 3.5 Appearance of ICGNP produced with different S/NS ratio, after lyophilization. The effect of S/NS ratio on %LC could be observed clearly as the increase in color density as more ICG was trapped inside nanoparticles with increasing %LC.

3.3.2 Effects of ICG concentration on nanoparticle characteristics

In order to examine the effects of initial ICG concentration in formulation on various nanoparticle characteristics, S/NS ratio was maintained at 1/3 with a fixed 10 mg/mL for PLA concentration. The results were summarized in Table 3.5.

Nanoparticle size was observed to be unrelated to initial ICG concentration as no significant difference was noted among different formulations. On the other hand,

Table 3.5
Effects of ICG concentration on nanoparticle characteristics.Each formulation contains 10 mg/mL PLA, S/NS ratio = 1/3, n=3.

ICG concentration (μM)	Size (nm)	EE (%)	LC(%)	Yield (%)
30	302.8±1.1	1.6±0.8	0.04±0.01	18±1
50	310.1±3.5	3.9±1.3	0.1±0.02	27.3±6
80	311.4±1.7	5.2±1.7	0.2±0.01	31.3±9
110	336±18	3.5±1.2	0.22±0.04	26.7±5
150	283.4±7	3.1±0.5	0.27±0.02	24.7±8
200	279±8.3	3.1±0.3	0.33±0.03	29.3±1
500	299.6±22.6	2.3 ±0.1	0.57±0.01	42.4±2
1000	294.1±7.2	0.3±0.1	0.25±0.03	18.4±2

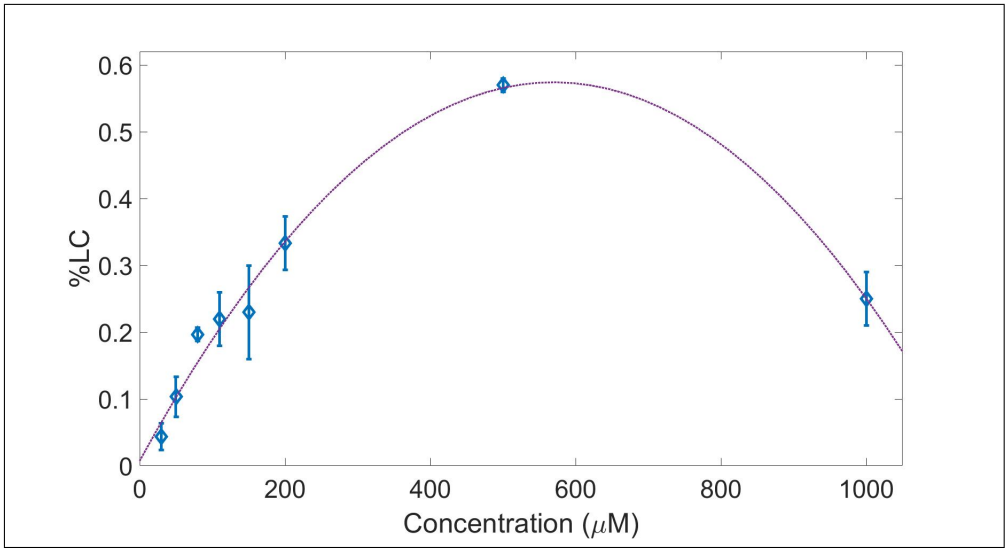

Figure 3.6 The effect of increasing ICG concentration on the loading capacity of nanoparticles produced. 500 μM initial ICG concentration caused a statistically significant increase in the amount of ICG encapsulated. A sharp decline in %LC was observed with further increase in ICG concentration.

loading capacity was affected substantially with increasing dye concentration. This effect can be observed in Figure 3.6. The increase in loading capacity as ICG concentration increased to 500 μM was statistically significant. However, further increase in concentration resulted in a drastic loss of loading capacity.

3.3.3 Characterization of ICGNP

In light of these results, the formulation summarized in Table 3.6 were chosen to be used to produce nanoparticles with highest loading capacity, good yield and optimal size. The raw suspension of nanoparticles produced by aforementioned formulation exhibited a bimodal size distribution with the larger nanoparticle population centered around 300 nm in diameter and a smaller population of aggregates with an approximate diameter of 700 nm, as observed in left side of Figure 3.7. The aggregates were separated by centifugation at $1500g$ for 15 min, which resulted in well defined nanoparticles with a narrow size distribution (PDI: 0.05 ± 0.04).

Table 3.6
Formulation used to produce nanoparticles to be used in phototherapy experiments.

Polymer concentration	10 mg/mL in acetone
ICG concentration	500 μM in 2% aqueous PVA
S/NS ratio	1/3

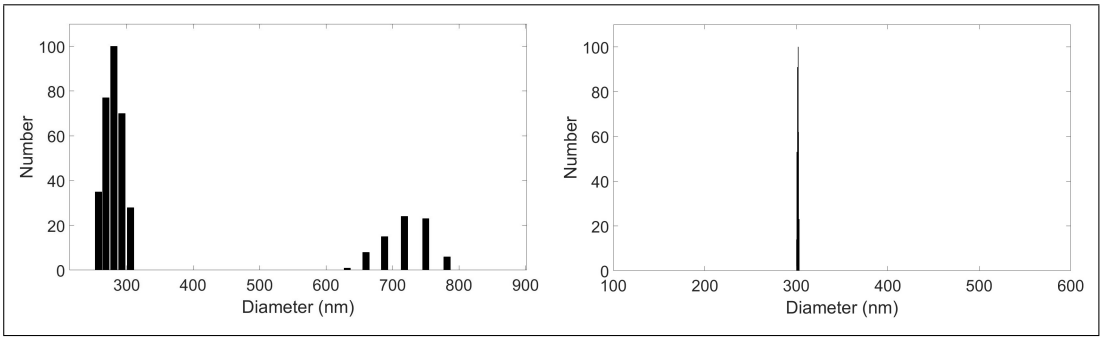

Figure 3.7 The size distributions of nanoparticles, with aggregates (left) and after aggregates were removed by centrifugation (right).

ICGNP were observed to have an average size of 300.58 ± 20 nm in diameter, with a zeta potential of -14.27 ± 0.02 mV. SEM and STEM images revealed solid nanospheres with smooth surfaces and low polydispersity, as observed in Figure 3.8. 1 mg of nanoparticles were found to have an equivalent ICG concentration of 8.3 ± 0.8 μM upon resuspension in 1 mL of liquid.

The amount of ICG released from ICGNP under physiological conditions were

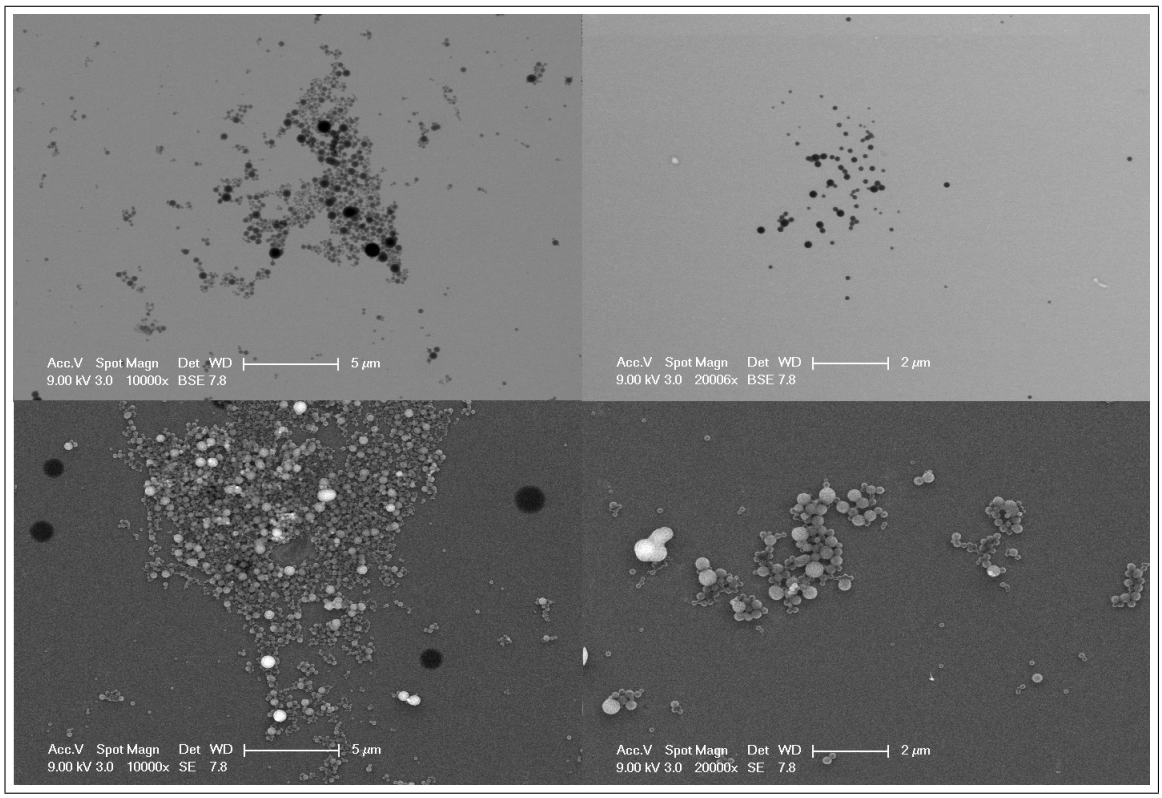

Figure 3.8 STEM (upper row) and SEM (lower row) micrographs of nanoparticles indicating spherical nanoparticles.

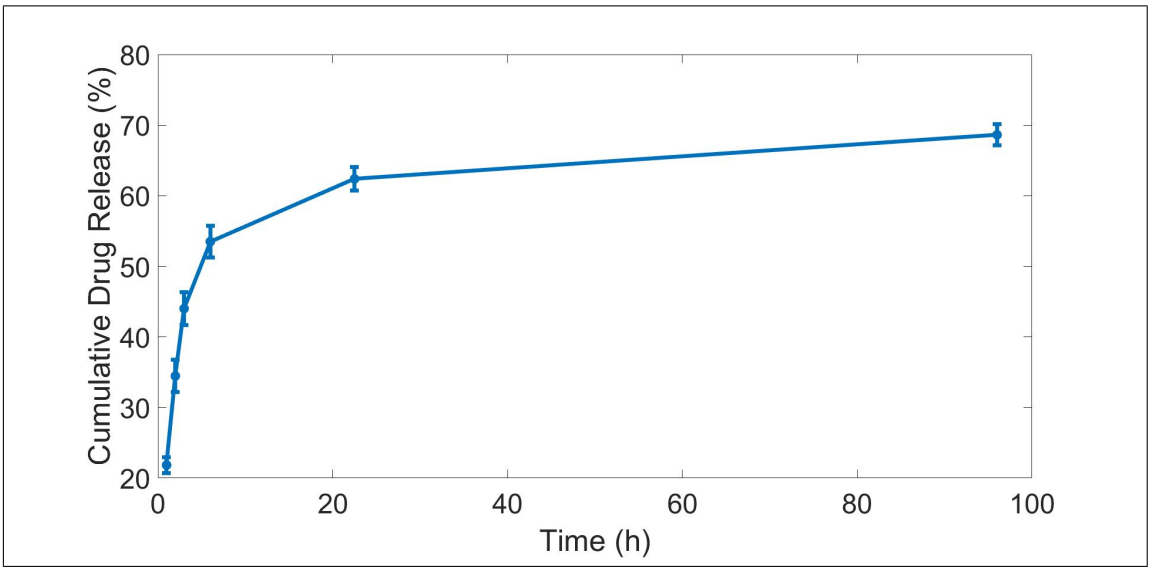

Figure 3.9 ICG released from ICGNP upon incubation in PBS at 37 °C. A quick release phase was evident for the first 4-5 hours, followed with a slower release lasting for several days.

studied in drug release experiments. The results were described in Figure 3.9. Approximately 50% of ICG encapsulated in ICGNP was observed to be released in the first 4 hours of incubation, while up to 70% of ICG was released in the long term. Nevertheless, at least 30% of initial ICG amount was observed to be retained even after long term incubation.

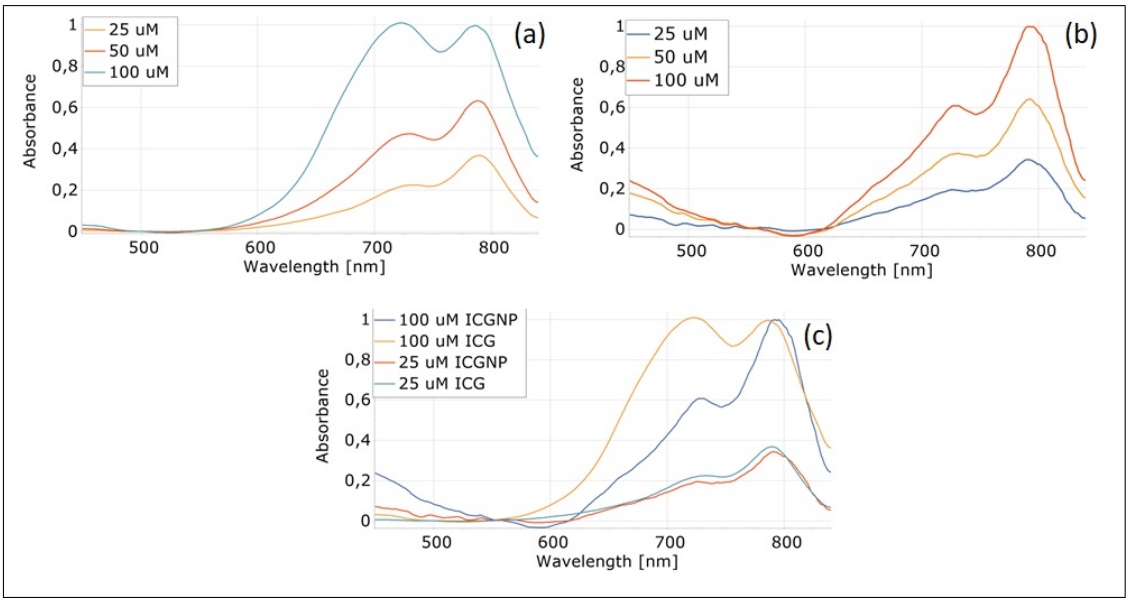

Figure 3.10 Absorption spectra of (a) free ICG and (b) ICGNP at different concentrations in cell culture media (c) Comparison of absorption spectra of free ICG and ICGNP at identical concentrations. Aggregate formation in free ICG was evident as the formation of a prominent new peak around 700 nm, whereas in ICGNP this peak was less emphasized.

Optical spectra of both ICG and ICGNP in cell culture medium at different concentrations were plotted in Figure 3.10.The aggregation of ICG was indicated by the formation of a new absorption peak at 720 nm at higher concentrations. This peak was also present in ICGNP spectra, albeit at a much lower intensity, which demonstrate less aggregation of ICG in encapsulated form. At identical concentrations, free ICG exhibited slightly red-shifted peaks than ICGNP. Furthermore; absorption spectra of ICGNP were shown to retain their shape as concentration increased, whereas in free ICG spectra, new peak formation implying ICG aggregation was observed.

3.3.4 Demonstration of ROS and heat production capabilities of ICGNP

ICGNP was also characterized in terms of its ROS and heat production capability in order to determine its suitability as a phototherapy agent. ROS production was monitored indirectly by utilizing the absorption reduction on DPBF in presence of singlet oxygen. DPBF could only be dissolved in organic solvents (ethanol in this instance), yet ICGNP could not be suspended in ethanol at concentrations higher than 10 μM therefore an ethanol/water mixture (4:1, v:v) was utilized. Samples containing different concentrations of ICG or ICGNP were prepared in spectrophotometry cuvettes and irradiated in 15 s cycles. DPBF absorption was measure before and after every irradiation and obtained values were plotted against time. Free ICG was observed to induce more DPBF bleaching, demonstrating more singlet oxygen production, as seen in Figure 3.11a. However, ICG at all concentrations tested underwent faster photobleaching than ICGNP and were unable to continue ROS production after 30 s of irradiation. On the other hand, ICGNP was observed to exhibit a less pronounced ROS production, indicated by a slower bleaching of DPBF, displayed in Figure 3.11b. Although the overall ROS production by ICGNP were less than that of free ICG, ICGNP were observed to continue ROS production for periods twice longer than free ICG.

The amount of heating in the cell culture medium as a result of laser light absorption due to free ICG and ICGNP were also measured. The samples were prepared in spectrophotometry cuvettes by dispersing ICG or ICGNP at predetermined concentrations in cell culture medium. Samples were irradiated at 1 W/cm^2 for 400s. The increase in temperature was measured with the help of a T-type thermocouple immersed in liquid and recorded every 20 s. The results were summarized in Figure 3.12. No significant heating was observed in blank cell culture medium ($\Delta T_{max} = 3.5$ °C). At the highest concentrations tested, both ICG ($\Delta T_{max} = 48$ °C) and ICGNP($\Delta T_{max} = 50$ °C) were capable of producing significant heating effect, reaching a maximum of 74 °C. Cooling started at around 140, 180 and 300 s (for concentrations 10, 30 and 50 μM, respectively) as photobleaching caused a significant decrease in the absorption.

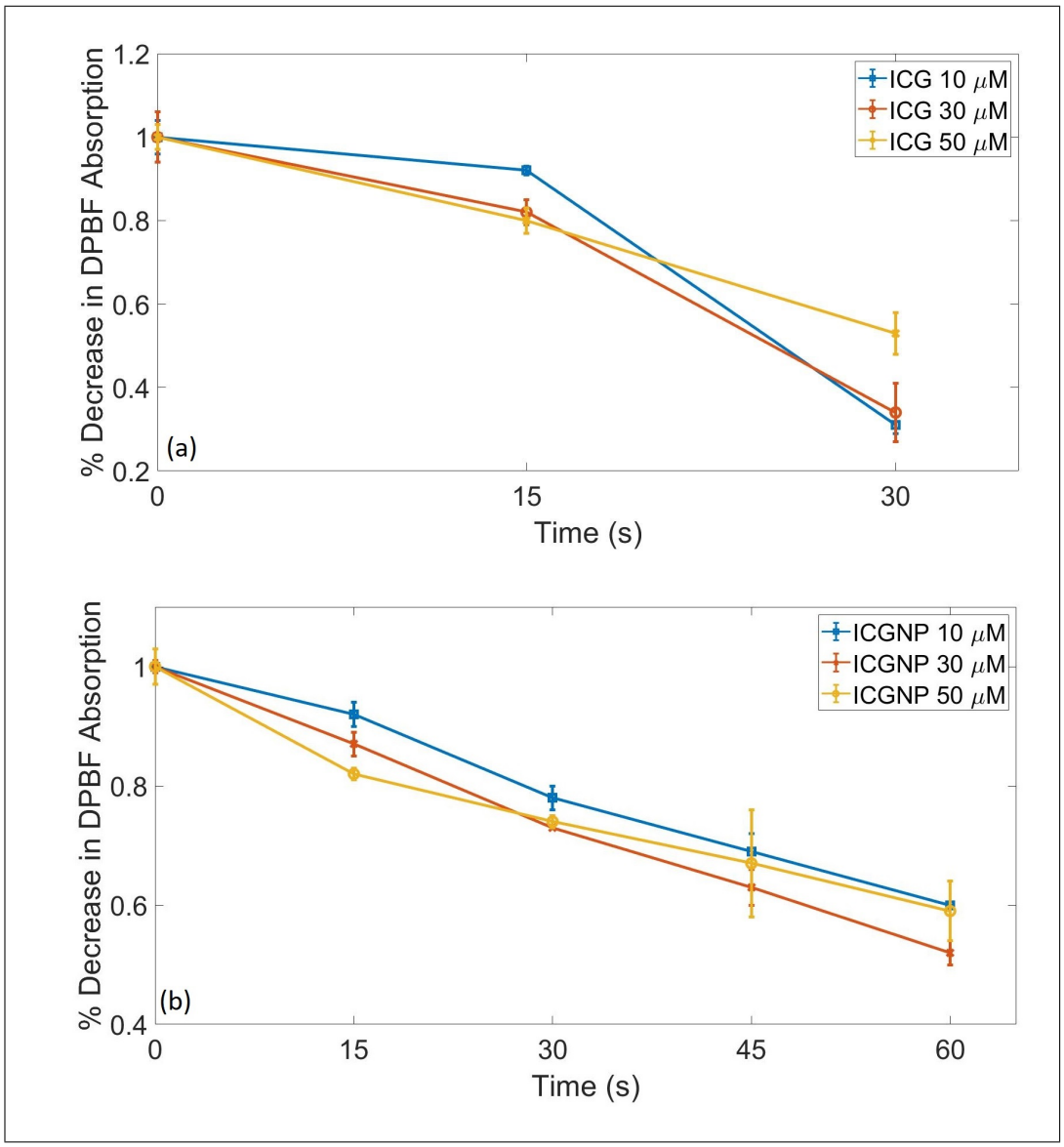

Figure 3.11 ROS production measured as the absorption decrease of DPBF a)free ICG b) ICGNP.

3.4 Discussion

Two characteristics of ICGNP are significant in determination of their suitability for phototherapy. The first one is the average nanoparticle size, which determines the fate of the nanoparticles upon administration. Although particles as large as 1 μm can interact with cells and be internalized in vitro [83], nanoparticles larger than 300-400 nm were known to be cleared rapidly from circulation due to their interactions with mononuclear phagocytic system (MPS). Nanoparticles of sizes in between 150 and 300

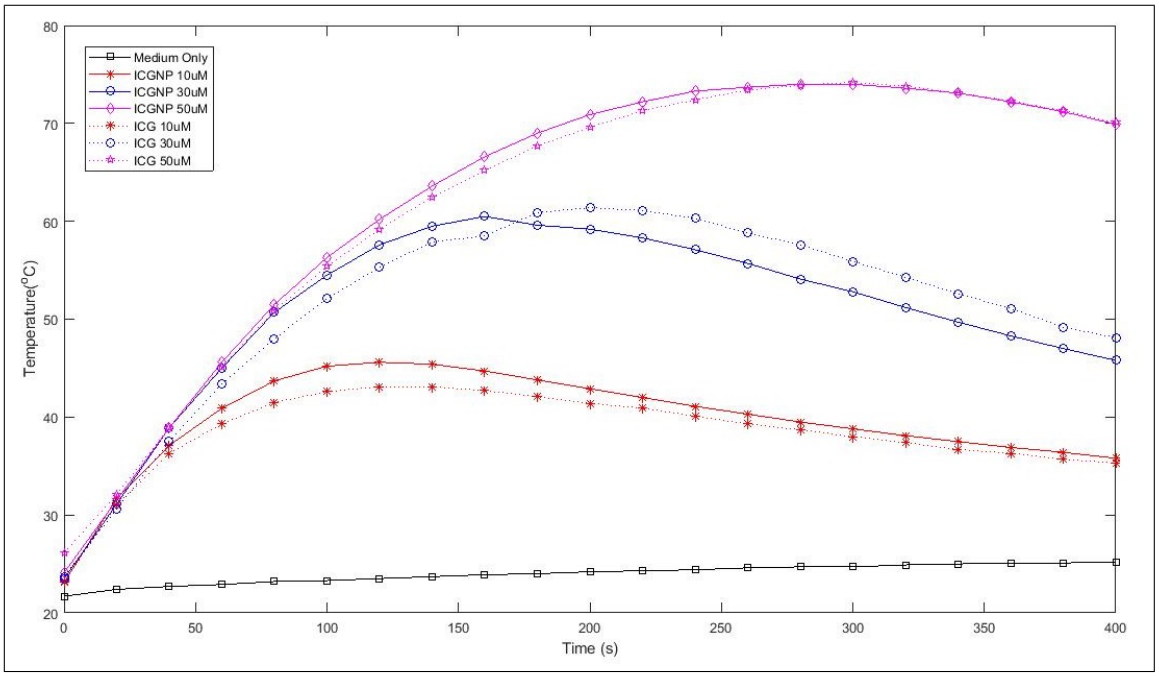

Figure 3.12 Temperature increase upon irradiation by 809 nm, 1 W/cm^2 in cell culture medium supplemented with free ICG and ICGNP at different concentrations.

nm accumulates in the liver and the spleen, while smaller nanoparticles (30-150 nm in diameter) can be found in the heart, the kidneys and the stomach [49]. Furthermore, nanoparticles smaller than 50 nm were shown to clear rapidly from the tumor [84]. Therefore, an optimal size interval exists for nanoparticles.

The second important characteristic is the loading capacity, which determines how much drug is encapsulated per unit weight of nanoparticle. PLA nanoparticles are generally accepted to be safe; for example, on Caco-2 cells no significant toxicity was observed upon incubation with PLA nanoparticles up to 300 μg/well concentration [85]. However, ICG exhibits low singlet oxygen quantum yield [10, 17] and requires high concentrations to be effective as a phototherapeutic agent. In order to deliver high concentrations of ICG using PLA nanoparticles, good loading capacity is required. Therefore, the smallest nanoparticles with the highest drug content was aimed.

In this study, polymeric nanoparticles encapsulating ICG were produced via nanoprecipitation in order to minimize the use of toxic solvents and extensive experimental setup. Nanoparticles were produced instantaneously upon solvent phase

injection into non-solvent phase of larger volume, as observed in an increase of mixture turbidity. In this part, two conditions must be met for nanoparticles to be formed: the solvent phase must be a dilute polymer solution and, the solvent and non-solvent phases must be miscible. Customarily, non-solvent phase is chosen as distilled water as to minimize the use of potentially toxic solvents. Non-solvent phase then should be chosen from solvents of the polymer that are also miscible with water. Among possible candidates acetone is widely used, and is known to produce smaller nanoparticles than tetrahydrofuran [62]. Furthermore, no significant difference in terms of size or yield is observed between nanoparticles produced using acetone or DMSO [59]. Therefore, the solvent/non-solvent system utilized in this study was chosen to be acetone/distilled water.

Polymer concentration is another important parameter that determines the characteristics of the nanoparticles produced. A dilute polymer solution is required for this process, and concentrations up to 33 mg/mL were reported in literature. Preliminary experiments (reported in Appendix) with concentrations ranging from 5 to 15 mg/mL have shown that increasing polymer concentration causes an increase in nanoparticle size and causes more aggregates to be formed, which in turn, reduces nanoparticle yield [61,64]. Furthermore, optimal results in terms of particle size were reported at 10 mg/mL polymer concentration previously, therefore 10 mg/mL PLA was used in this study as well [59].

Size control parameters for nanoprecipitation technique also includes surfactant concentration in non-solvent phase. PVA, which is widely used as a stabilizer, was utilized in this study at a concentration of 2%. Increasing PVA concentration was reported to cause a decline in nanoparticle size up to 2- 4 % concentration range, however; further increase was shown to induce an increase in particle size [51, 59, 86–88]. This effect can be explained by the increased viscosity of non-solvent phase with increased PVA concentration, which causes particle aggregation. Initial drug concentration, on the other hand, reported to have no effect on nanoparticle size for ICG loaded PLGA nanoparticles [66, 73, 80].

The effect of S/NS ratio on nanoparticle size, yield and drug loading capacity was investigated by changing S/NS ratio in a range, from 0.05 to 0.5, with ICG and PLA concentrations kept constant. The results in particle size exhibited an increasing trend, although not statistically significant, with increasing S/NS ratio, which was in agreement with literature [59]. This propensity for larger nanoparticle diameters with higher S/NS ratios was speculated to be due to increased viscosity of the final solution which hinders the diffusion process. Furthermore, higher S/NS ratio formulations were observed to have lower yields, due to more aggregates being formed. These aggregates caused measured nanoparticle effective diameters to be larger than expected, which was attributed to the indirect nature of DLS method. In a typical DLS setup, laser light is used to illuminate the sample containing particles, which scatter the light. The scattered light and its fluctuations due to the Brownian motion of particles are analysed and used to calculate the hydrodynamic diameter via Stokes-Einstein equation [89]. Since larger particles cause more prominent scattering, even a smaller population of large particles can cause a significant increase in the calculated effective size. These larger particles were observed in size distribution detail of DLS as a small population. Elimination of these aggregates via centrifugation yielded well defined nanoparticles with low PDI.

In order to increase the amount of drug loaded in nanoparticles, different methods were employed and reported in the literature. At fixed drug concentration, drug loading was expected to increase with increasing polymer concentration or S/NS ratio [87]. Our results suggested a limit on the %LC increase obtained by increasing S/NS ratio, as observed in Table 3.4. Increasing polymer concentration was not utilized in this study, since it was known to produce larger nanoparticles [59,64,73]. Furthermore, this approach was reported to have no effect on the %LC as it increases only %EE [64]. Another attempt to increase %LC was done by increasing ICG concentration in formulation. For PLGA nanoparticles, a fixed capacity to encapsulate ICG was reported previously utilizing ICG concentrations of 55, 270 and 540 μM at 1/5 S/NS ratio [64]. In comparison, increasing S/NS ratio to 1/3, better ICG encapsulation at 500 μM was achieved (0.57% compared to 0.29% in %LC) in this study. Further increase in ICG concentration was observed to cause a decrease in %LC.

Increasing ICG concentration to 1000 μM also caused a sharp decline in nanoparticle yield, which could be due to the amphiphilic nature of ICG that caused rapid migration of ICG molecules to aqueous phase during precipitation, disturbing the formation of nanoparticles. Furthermore, the relatively low %LC could also be attributed to the water-solubility of ICG, causing ICG molecules to swiftly partition into the aqueous phase during precipitation of nanoparticles [90].

Nanoparticles produced with proposed parameters of 10 mg/mL PLA, 500 μM ICG, at 1/3 S/NS ratio were observed to be spherical, approximately 300 nm with low PDI and had a zeta potential of -14 mV, which was deemed advantageous since nanoparticles with slightly negative surface charge were reported to have the longest half-lives in circulation [91] and was in agreement with the literature [68, 72, 73]. ICG release from ICGNP followed a biphasic pattern, first with quick release (50% of ICG in 4 hours), followed with a slow release of additional 20%, similar to previous reports of PLGA nanoparticles [64,66]. The biphasic pattern could be interpreted as a result of ICG distribution in PLA matrix. ICG molecules closer to the surface of the nanoparticles were released in the burst release phase, while the sustained release phase is due to the slow diffusion of ICG molecules deeper inside PLA matrix [68, 92].

Phototherapeutic effect provided by ICGNP could originate from its capability to produce singlet oxygen as well as heat upon irradiation. Singlet oxygen production of ICGNP was confirmed via absorption reduction of DPBF and compared to free ICG. Although both ICG and ICGNP cause a decrease in DPBF absorption, indicating singlet oxygen production, ICG provided significantly more singlet oxygen compared to ICGNP (70% reduction in DPBF absorption by ICG, compared to 25% reduction by ICGNP in 30 s irradiation). However; free ICG was observed to photobleach completely at the end of 30 s irradiation period (absorption peak of ICG at 800 nm disappeared), whereas ICGNP was capable of prolonged singlet oxygen production for up to 60 seconds.Nanoparticle encapsulation appeared to delay ICG decomposition, providing some optical stability at the cost of lower singlet oxygen quantum yield. Moreover, singlet oxygen quantum yield of ICG was observed to be concentration dependent, observed as the relatively lower singlet oxygen production of 50 μM ICG, compared to lower

concentrations. Such a concentration dependent manner was not observed in ICGNP, which provided stable singlet oxygen production independent of concentration. Singlet oxygen production in similar nanoparticles were also reported in literature in which ICG containing nanoparticles were utilized as fluorescence nanoprobes [74, 79, 82].

Photothermal effect of ICGNP was demonstrated as the temperature increase in the medium. Induction of hyperthermia was reported to increase the efficiency of chemotherapy, therefore the ability to generate heat upon irradiation was favorable for dual drug delivery systems which incorporate a chemotherapeutic agent [71, 72, 81, 93]. ICGNP was shown to cause temperature increase in media sufficient to induce hyperthermia, even at the lowest dose employed. However, after 2.5 min the medium started cooling, due to the irreversible degradation of ICG. The rate at which degradation took place appeared to be related to the irradiance level. For similar nanoparticles at an ICG-equivalent concentration of 20 μM, cooling was reported to start after 6 min at 0.75 W/cm^2 irradiance [93] and after 2 min at 1.5 W/cm^2 [79]. Compared to these results, starting point of cooling at 2.5 min encountered in this study was expected. In culture medium, temperatures as high as 70 °C could be obtained at 50 μM concentrations, which was sufficient to inactivate cells in a short time span.

3.5 Conclusion

ICGNP was prepared via nanoprecipitation, and adequate encapsulation of ICG in PLA nanospheres were demonstrated. Characteristics of the nanoparticles were in agreement with the literature on ICG-PLGA and on blank PLA nanoparticles. ICGNP were observed to have suitable size, morphology and surface charge to be used in cell culture. Furthermore, some level of protection of ICG from aggregation and degradation due to encapsulation was observed. ICGNP were also demonstrated to generate heat and produce singlet oxygen upon laser irradiation. As a result, ICGNP were deemed suitable to be used as a phototherapy agent on cancer cells.

4. PHOTOTHERAPEUTIC EFFECTS OF ICG LOADED PLA NANOPARTICLES ON PC-3 CELLS

4.1 Introduction

ICG-incorporating nanoparticles of various materials were reported in the literature with varying degrees of phototherapeutic effects. Among those, PLGA based nanoparticles were the closest type to the ICGNP nanoparticles proposed in this study. Most of studies involving ICG-encapsulating PLGA nanoparticles incorporated a chemotherapeutic agent (generally DOX) as well. It has been previously demonstrated that ICG application in conjunction with DOX provides synergistic effect when laser induced hyperthermia was present [94]. Therefore ICG was generally used to provide mild hyperthermia in order to increase the efficiency of DOX chemotherapy.

The phototherapeutic results obtained *in vitro* with various ICG-PLGA nanoparticles are summarized in Tables 4.1 and 4.2.

Table 4.1
Studies about the effects of polymeric nanoparticles encapsulating only ICG.

Nanoparticle	Cell Line	Irradiation Parameters	Treatment Results	Notes	Reference
PLGA-ICG	P388-D1 (macrophage)	805 nm; 100 J/cm^2	@50μM; 30% viability with free ICG, 60% viability with PLGA-ICG	Very low singlet oxygen quantum yield ($\Phi_{^1O_2} \approx 0.002$); no thermal data	[66]
PLGA-ICG	MCF-7; MDA-MB-231 (mammary carcinoma)	808 nm; 6 W/cm^2; 5 min	@25μM; $\approx$ 50% viability for free ICG on both cell line; $\approx$ 45% viability for PLGA-ICG without targeting; $\approx$ 5% viability with targeting	Comparable photothermal properties ($\Delta T_{max} = 45$°C for both) and singlet oxygen production with both free ICG and PLGA-ICG	[68]
mPEG-b-C18-TPGS-PLGA-ICG	MCF-7 (mammary carcinoma)	808 nm; 1W/cm^2; 5 min	@15μM; 60% viability for free ICG; $\approx$ 10% viability for mPEG-b-C18-TPGS-PLGA-ICG	Better photothermal effect than free ICG	[95]
PLGA-lecithin-PEG-ICG	BxPC-3 (pankreatic carcinoma)	1.6W/cm^2; 5 min	@103μM; 5% viability for PLGA-lecithin-PEG-ICG	@25μM $\Delta T_{max} = 57$°C (56°C for free ICG)	[69]
PLGA-ICG	B16-F10 (melanoma)	786 nm; 0.22 W/cm^2; 1.1 J/cm^2	@11nM 78% viability; @22nM 76% viability	-	[80]

Table 4.2
Studies about the effects of polymeric nanoparticles encapsulating ICG along with other anticancer agents.

Nanoparticle	Cell Line	Irradiation Parameters	Treatment Results	Notes	Reference
PLGA-ICG-R848	RM9; PC3; LNCaP; DU-145 (prostate carcinoma)	808 nm; 1 W/cm^2; 10 min	$\approx$ 10% viability; concentration non-specified	$\Delta T_{max} \approx 10$°C in tumor models	[75]
PLGA-chitosan-CP-ICG	SKOV3 (ovarian carcinoma)	808 nm; 1528 J/cm^2	@150$\mu M \approx 5\%$ viability	$\Delta T_{max} = 24.7$ °C; singlet oxygen production demonstrated via fluorescent probe	[70]
PLGA-DTX-ICG	U87MG (glioblastoma)	808 nm; 2.5W/cm^2; 5 min	@12μM 30% viability	$T_{max;NP}$=53°C; $T_{max;ICG}$=56°C; intracellular ROS production confirmed	[82]
PLA-mPEG-DOX-ICG	MDA-MB-231 (mammary carcinoma)	808 nm; 0.3W/cm^2; 10 min	@206nM $\approx$ 30% viability; with no significant improvement with concentration increase	$\Delta T_{max} = 10$ °C; increased DOX efficiency due ICG-PTT	[81]
PLGA-DOX-ICG	EMT-6 (mammary carcinoma)	808 nm; 1.5W/cm^2; 8min	same amount of cell viability with free ICG without DOX at all concentrations tested	$\Delta T = 20$°C; same as free ICG	[79]
PLGA-DOX-ICG	SKOV3 (ovarian carcinoma)	808 nm; 6.7 W/cm^2; 3.5 min	@5μM sufficient hyperthermia to increase DOX cytotoxicity was observed	T_{max}=43°C @6.2μM ICG	[71, 72]

Majority of the studies involving ICG phototherapy utilized a diode laser operating at 808 nm, although irradiation at 786 nm and 805 nm were encountered as well. However, in terms of irradiance and fluence, a remarkably wide range was reported (as low as 1.1 J/cm^2; as high as 1800 J/cm^2), possibly due to the different cell lines utilized [68, 80]. ICG-equivalent concentrations also varied notably (from nanomolar range to hundred micromolars) [70, 80]. Even though ICG was regarded as minimally toxic in itself, a separate dosimetry study for each cell line to be studied was evidently required.

Reported cell viability inhibition upon irradiation values exhibited considerable variation among studies. For example, Gomes et al. reported PLGA-ICG nanoparticles to be less effective than free ICG on P388-D1 cells at identical concentrations. This could be a result of significantly large nanoparticles utilized ($\approx 800nm$, which would delay singlet oxygen and heat diffusion. Indeed, extremely low values of singlet oxygen quantum yield was observed with this type of nanoparticles, and the photocytotoxicity observed was interpreted as a result of radical formation. No data on thermal changes occurred was presented, making it impossible to infer whether the cell death was due to radical species or hyperthermia [66].

On the other hand, Lee et al. reported the same amount of singlet oxygen production and comparable thermal effects with PLGA-ICG compared to free ICG. Cell viability inhibition for nanoparticles were reported to be slightly better than free-ICG without targeting. With targeting, nanoparticles caused almost complete cell eradication. Nanoparticles employed in this study was suitably small and the fluence was significantly larger than what was used by Gomes et al. Combination of these two difference might be the reason behind significantly different results obtained [68].

In terms of photothermal conversion capability, conflicting results were presented as well. Tang et al. reported slightly diminished heating with PLGA-ICG where 6.2 μM PLGA-ICG produced same amount of heating with 5 μM free ICG, which was assumed to be a result of PLGA shell delaying heat diffusion [72]. To the contrary, several studies documented encapsulated-ICG being as good as free ICG in

terms of temperature rise under same conditions [68,69] or even exhibit better heating capabilities compared to free ICG, explained as a result of increased stability of ICG molecules [95].

For nanoparticles encapsulating another anticancer agent along with ICG, DOX was a popular choice. Several studies reported that ICG-mediated moderate temperature increase increased the efficiency of DOX-mediated cell death [71,72,79,81]. Since the main objective in these studies were to cause mild hyperthermia (T_{max}=43°C), ICG concentrations utilized were kept to a minimum and its effects other than hyperthermia-induction were not examined. Therefore, reported efficiency for these platforms were the result of more than one anticancer agent. Although ICG were reported to be included as a photothermal and photodynamic agent, effects of solely ICG-encapsulating nanoparticles were not investigated thoroughly. Singlet oxygen production via ICG was established in some of these studies, but its contribution to overall cell viability inhibition was not studied.

In this study, ICGNP were tested on PC-3 cells in order to determine the effects of encapsulation on the photothermal and photodynamic activity of ICG. The results were compared to free ICG in order to determine any significant improvement or deterioration arising from encapsulation.

The aim of the second part of this study is to evaluate the anticancer efficiency of ICGNP and to attempt to determine the dominant cell killing effect.

4.2 Materials and Methods

All cell culture reagents were purchased from Biosera (Nuaille, France), NaN_3 was purchased from Sigma-Aldrich (Darmstadt, Germany). PC-3 (ATCC CRL-1435) cells were cultured in RPMI-1640 medium supplemented with 10% fetal bovine serum (FBS) and 1% penicillin-streptomycin, in 25 cm^2 flasks, at 37°C in a humidified 5% CO_2 atmosphere. Fresh culture medium was provided at least twice a week and the

cells were subcultured right before reaching confluence.

Cells were detached using 0.25% (w/v) trypsin/EDTA solution, counted with the help of a hemocytometer, seeded at a density of 10^4cells/well in polystyrene 96 well plates and incubated overnight to ensure proper adherence.

4.2.1 Effect of laser light on cell viability

The effect of only laser light on PC-3 cells were evaluated by irradiating the cells in blank medium. Culture medium in the plates prepared were renewed the next day after overnight incubation and the plates were irradiated at 1 W/cm^2 for intervals of 50, 100, 200, 400 and 600 s, which equals to fluencies 50, 100, 200, 400 and 600 J/cm^2, respectively. Cell were incubated overnight after irradiation and the next day culture medium was replaced with medium supplemented with 10% MTT solution (5 mg/mL in PBS) and incubated for another 3h. Formazan crystals formed by viable cells during the incubation were dissolved in DMSO and absorbance at 570 nm was determined using a microplate reader(Bio-Rad iMark, CA, USA).

4.2.2 Dark toxicity of ICGNP

The dark toxicity of free ICG on PC-3 cells had been investigated previously [10] and it was established that ICG was not toxic for PC-3 cells in the concentrations used in this study, in dark. In order to determine the dark toxicity of ICGNP lyophilized nanoparticles were re-suspended in cell culture medium at ICG equivalent concentrations of 10 to 50 muM. Culture medium in plates were changed with ICGNP supplemented medium and plates were incubated for 2h for cells to internalize nanoparticles. After incubation; each cell was emptied, washed thrice with PBS, supplied with complete cell culture medium and incubated overnight. Cell viability was assessed using MTT test as detailed before.

4.2.3 Phototoxicity tests

In this part, the decline in cell viability after treatment with either free ICG or ICGNP at certain concentrations followed by laser irradiation was examined. Cell culture plates were prepared as the same with dark toxicity experiments. For free ICG groups, a stock solution of ICG at 1 mM concentration was prepared in distilled water, since ICG solubility in culture medium is very low, and diluted with medium to appropriate concentrations. ICGNP were directly suspended in culture medium by vortexing at ICG equivalent concentrations of 10, 30 and 50 μM. Cells were incubated with either free ICG or ICGNP supplemented medium for 2h. After incubation, wells were emptied, washed thrice with PBS and fresh culture medium was added. Subsequently, plates were irradiated with laser light (1 W/cm^2, for a duration of 200 or 600s, up to a total of 200 or 600 J/cm^2), before they were incubated further overnight. Cell viability was assessed using MTT test as detailed before.

4.2.4 Photothermal effects on cells

The increase in temperature caused by laser irradiation was observed with the help of a T-type thermocouple (MT-29/1, Physitemp, NJ, USA). PC-3 cells seeded on a 96-well plate were incubated with free ICG or ICGNP at concentrations 10, 30 and 50 μM for 2h, washed thrice with PBS and supplemented with fresh culture medium. Thermocouple needle was inserted in the well under laser irradiation at 1 W/cm^2 and the temperature was recorded for 360s at 20s intervals.

4.2.5 Photodynamic effects in the presence of a singlet oxygen quencher

The effect of singlet oxygen produced by free ICG and ICGNP on cell viability was investigated utilizing a singlet oxygen quencher NaN_3. In order to determine the sufficient concentration of NaN_3 to quench the singlet oxygen produced by ICG, 50μM ICG containing DPBF solutions were added NaN_3 at concentrations 10 and 50 mM.

The samples were irradiated at 100 mW/cm^2 for a total of 80s and the decrease in DPBF absorption was measured. The recorded absorption reduction plotted against time was used to determine the efficiency of NaN_3 in quenching singlet oxygen. NaN_3 was used in the same concentrations in cell culture in order to determine how much of cell death was due to singlet oxygen produced by ICG and ICGNP. PC-3 cells were seeded on a 96-well plate as previously described and cells were incubated with 0 and 50 μMICG or ICGNP along with 10 and 50 mM of NaN_3 for 1 h. Cells were washed thrice with PBS after incubation, irradiated at 600 J/cm^2 fluence and incubated overnight. MTT test for cell viability was carried out the next day.

4.2.6 Statistical analysis

All experiments were conducted as three independent experiments containing at least three technical replicates. Results obtained from MTT test were normalized according to the control group, setting control group viability to 1. Data were reported as mean ± standard deviation. Statistical analysis was performed using ANOVA followed by Tukey's test to determine the groups that differ statistically significantly. The level of significance was set at $p \leq 0.05$.

4.3 Results

4.3.1 Effect of laser light on cell viability

The effect of only laser light on the viability of PC-3 cells up to a fluency of 600 J/cm^2 at 1 W/cm^2 irradiance was investigated. Results were summarized in Figure 4.1. Fluences 100 and 200 J/cm^2 appeared to have a slight proliferative effect on cells, however this effect was not statistically significant. None of the irradiated groups exhibited any significant difference compared to control group therefore laser light only, at parameters used, was regarded as safe on PC-3 cells.

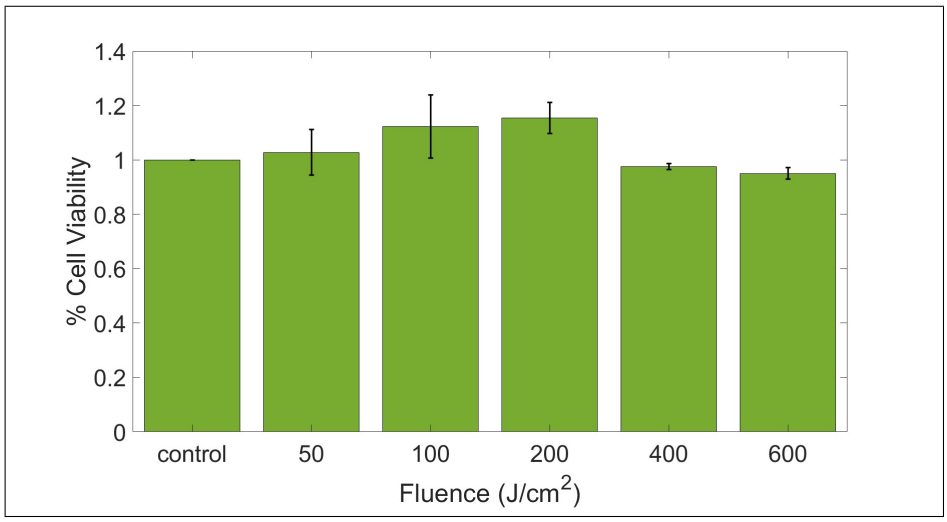

Figure 4.1 Effect of laser light on PC-3 cell viability at 1 W/cm^2.

4.3.2 Dark toxicity of ICGNP

Dark toxicity of free ICG on various cell lines including PC-3 was well analyzed previously [10] and concentrations used in this study was established as safe. Therefore, dark toxicity of only ICGNP was examined in this study, up to concentrations of 50 μM ICG equivalent. No significant difference between groups of different ICGNP concentrations and control were observed hence ICGNP up to 50 μM was considered safe.

4.3.3 Phototoxicity tests

Laser light irradiation at 1 W/cm^2 on cells incubated with ICG or ICGNP at various concentrations resulted in a decrease in cell viability. The decrease was statistically significant from control in all groups above 10 μM concentration, for both free ICG and ICGNP. Compared to each other at same concentration and fluence levels, ICG provided slightly more cell death, however no statistically significant difference in between groups of same concentration was observed.

Furthermore, comparing between groups of same concentration, higher fluency

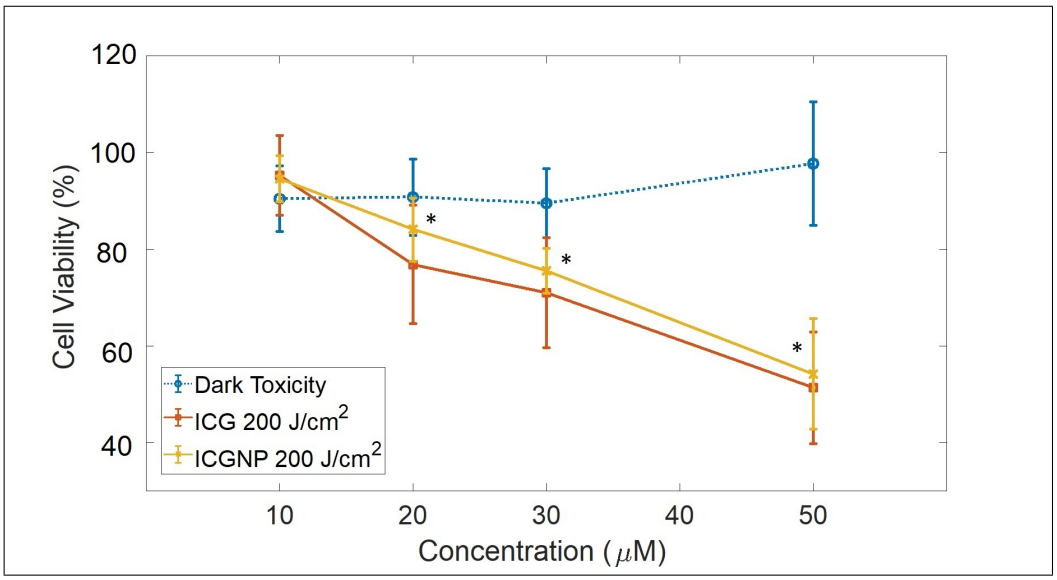

Figure 4.2 Phototoxic effect of ICG and ICGNP at 200 J/cm^2.Asterisk denote statistically significant difference at p≤0.05 level.

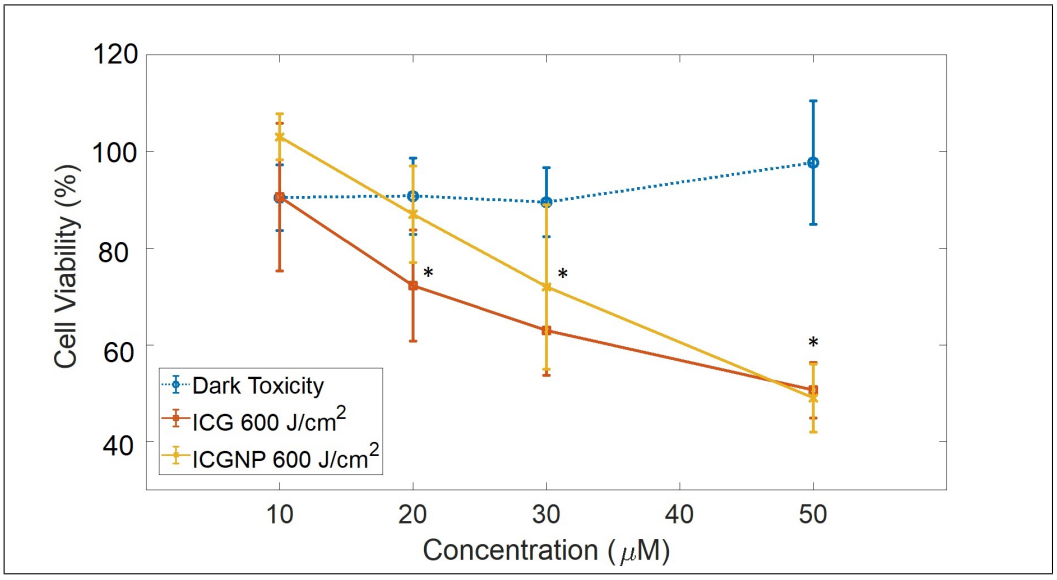

Figure 4.3 Phototoxic effect of ICG and ICGNP at 600 J/cm^2.Asterisk denote statistically significant difference at p≤0.05 level.

appeared to provide slightly better cell killing ability. However, this effect was not statistically significant and 200 J/cm^2 fluence provided approximately the same amount of decrease in cell viability as 600 J/cm^2. Cell viability was decreased to approximately 50% for both ICG and ICGNP groups at 50 μM concentration, with higher laser fluence providing slightly more cell death.

These results were presented in Figure 4.2 for 200 J/cm^2 and in Figure 4.3 for 600 J/cm^2 groups.

4.3.4 Photothermal effects on cells

The temperature change of the medium containing the cells under irradiation was recorded via a T type thermocouple needle. PC-3 cells, seeded on a 96-well plate and incubated with ICG or ICGNP at concentrations 10, 30 or 50 μM for 2 h were washed with PBS and irradiated (1 W/cm$^{2)}$ after supplemented with fresh medium. Temperature was measured and recorded at 20 s intervals during irradiation. Cells incubated in a blank medium (no ICG or ICGNP added) were used as a control. For control group, the recorded temperature increase reached to a maximum of approximately 9 °C ($\Delta T_{max} \cong 9$ °C). Increased amount of both ICG and ICGNP caused a significant heating effect on the culture medium, with no cooling recorded in the 360s irradiation duration. Even at the lowest concentration of 10 μM ICGNP was capable of reaching to a maximum of 42.8 °C in temperature, which was sufficient to cause devitalization in durations used in this study. The results were illustrated in Figure 4.4.

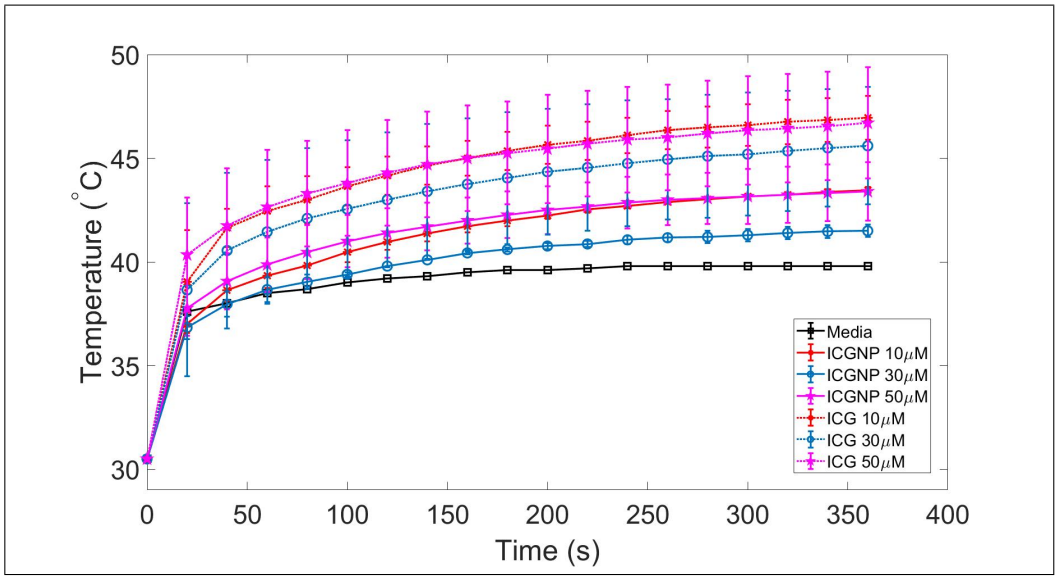

Figure 4.4 Temperature increase during irradiation (1W/cm^2) in cell culture plate.

4.3.5 Photodynamic effects in the presence of a singlet oxygen quencher

Both ICG and ICGNP suspended in cell culture medium were shown to produce singlet oxygen upon laser irradiation. In order to determine how much of the cellular death observed was due to singlet oxygen, a chemical that can trap singlet oxygen was used in conjunction with both ICG and ICGNP on PC-3 cells. Sodium azide, NaN_3, was utilized to this end since its known to be an effective singlet oxygen quencher [16]. The quenching effect of the concentrations utilized were first demonstrated in DPBF solutions incorporating 50 μM of ICG. Irradiation of the solutions yielded an expected DPBF absorption reduction for 0 mM NaN_3 groups which demonstrates the effect of the singlet oxygen produced. However, no absorption reduction was observed in groups containing 10 and 50 mM NaN_3, which prove the efficiency of NaN_3 in quenching singlet oxygen. These results were shown in Figure 4.5.

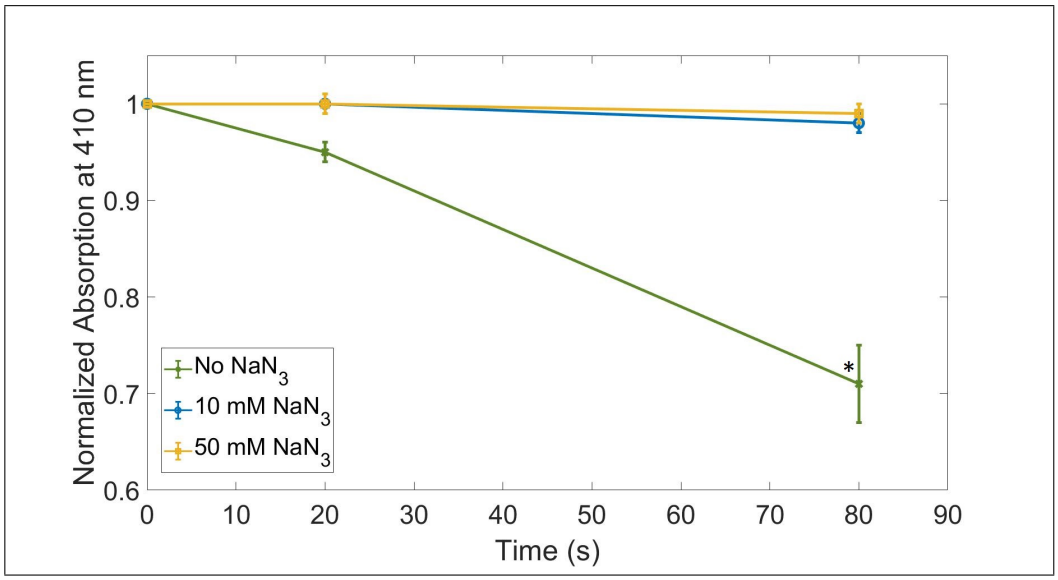

Figure 4.5 Singlet oxygen quenching capability of NaN_3 at concentrations 10 and 50 mM.Asterisk denote statistically significant difference at $p \leq 0.05$ level.

In the next part, the cellular toxicity of NaN_3 was evaluated at 10 and 50 mM concentration. Afterwards, NaN_3 supplemented medium was used to prepare ICG and ICGNP solutions and cells were incubated with these solutions for an hour. Irradiation took place at the end of the incubation period. Cell viability results were shown in Figure 4.6. Control groups containing 0, 10 or 50 mM NaN_3 were used to test

cellular toxicity (no laser irradiation) and exhibit no statistically significant difference in terms of cell viability. Therefore, concentrations used were regarded as safe. Cells irradiated after incubation with either ICG or ICGNP exhibit no difference in cell viability associated with NaN_3 concentrations. NaN_3 addition appeared to have no effect on the decrease of cell viability after irradiation.

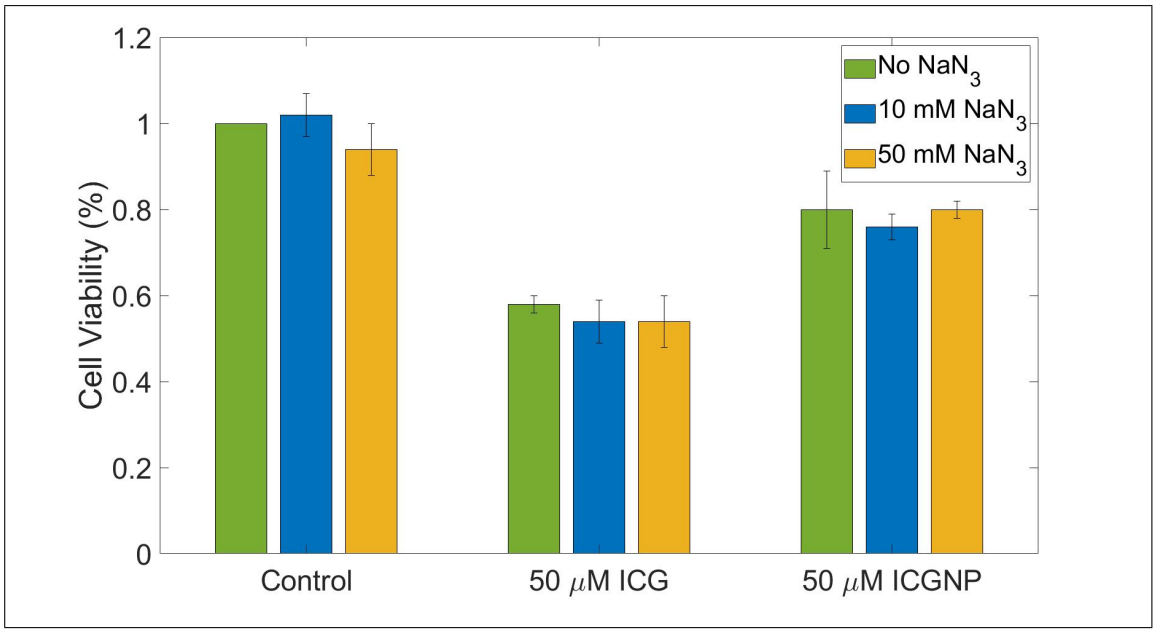

Figure 4.6 Effect of singlet oxygen quenching on cell viability after laser irradiation (600 J/cm^2).

4.4 Discussion

Phototoxic effects of ICGNP were evaluated in this part and results were compared to free ICG under same conditions. ICGNP was observed to have no significant dark toxicity at the concentrations used. Upon irradiation, both ICG and ICGNP were able to inhibit cell viability in a concentration dependent manner. No significant difference in cell viability was observed between ICG and ICGNP groups of same concentration, demonstrating ICGNP to be as effective as free ICG. Furthermore, increasing fluence at constant irradiation caused no statistically significant change in cell viability among groups of same concentration. The maximum temperatures reached with both 200 and 600 J/cm^2 appeared to be approximately same, with 600 J/cm^2 providing prolonged hyperthermia, which was assumed to provide improved cell viabil-

ity inhibition. This improvement, albeit not statistically significant, could be observed in cell viability inhibition.

Irradiation of PC-3 cells after incubation with ICG and ICGNP were shown to cause temperature increase sufficient to inhibit cell viability. While ICGNP was capable of causing 13°C temperature increase at most, free ICG performed better at $\Delta T_{max} \cong 17$ °C. The decrease in photothermal conversion capability could be due to encapsulating PLA matrix causing delayed heat diffusion [72]. Still, the maximum temperatures reached during irradiation were sufficient to inhibit cell viability as tumor cells would be killed in 5.5 min at 43 °C [96]. Temperature elevation characteristics observed was in agreement with the literature on ICG-mediated tissue heating, in which rapid heating during first 180-200 seconds were observed, followed by stable high temperature for prolonged duration [47]. The reported results for heating capabilities of free and encapsulated ICG in the literature are contradictory. Some studies reported diminished heating capabilities with ICG-PLGA nanoparticles [72], while others reported comparable heating capability to free ICG [97]. In another study, an increased photothermal conversion due to the slight redshift in absorbance spectrum following encapsulation of ICG was documented. This shift was explained to cause more efficient absorption of laser light since the peak shifted closer to irradiation wavelength, which in turn resulted in better photothermal efficiency than free ICG [93]. In view of these results, photothermal efficiency was assumed to depend strongly on nanoparticle characteristics.

ICGNP were shown to produce singlet oxygen upon irradiation. ROS production by similar nanoparticles were also demonstrated with the help of fluorescent ROS probes [74, 79, 82]. In order to examine the cell death resulting from increase oxidative stress, sodium azide was used as a singlet oxygen scavenger. Since NaN_3 was known to inhibit singlet oxygen production, cell viability was expected to increase in its presence if singlet oxygen was responsible for the majority of cell viability inhibition. This method was utilized previously by Bäumler et al. and Fickweiler et al. on ICG to confirm the cell killing effect of ICG under irradiation was,in fact, due to singlet oxygen production and therefore, photodynamic [12, 16]. However, in this study, NaN_3 addi-

tion to culture medium appeared to have no significant effect on cell viability, therefore photothermal activity seemed to be the dominant mode of cell inhibition. One possible explanation for this phenomenon was the use of high irradiances that caused photothermal effects to dominate over photodynamic effects. In previous studies that utilized NaN_3 to suppress the loss in cell viability, much lower irradiation schemes were used (48 J/cm^2 in Fickweiler and 30J/cm^2 in Bäumler). It was also possible that the phototoxicity of ICG might be a result of its own photooxidation by-products rather than the singlet oxygen it produced. Therefore, singlet oxygen produced inside the nanoparticles where NaN_3 could not quench, might be consumed by ICG molecules themselves to produce toxic degradation products which then cause cell death [19].

Polymeric nanoparticles of PLGA encapsulating ICG have been studied previously and provide a good basis for comparison. One of the earliest of these studies, conducted by Saxena et al, utilized ICG-PLGA nanoparticles of similar size (357 nm) with lower loading capacity (0.20%) than ICGNP on cell lines B16-F10 (melanoma) and C-33A (cervical cancer). Although the nanoparticles were used at minute ICG-equivalent dose of 22 nM, 24% of the cells were reported as eradicated after irradiation (1.1 J/cm^2, 808 nm). No information on the efficiency of free ICG under these parameters were reported [80]. The results obtained in this study, however; indicated more concentrated ICGNP suspensions (20 μM) were needed to provide approximately 20% cell eradication. Since the response to ICG-PDT was shown to vary with the cell line employed, the disparity in concentrations was attributed to the difference in the cell line.

Another ICG-PLGA nanoparticle system HER-2 targeted and coated with PEG, at a similar size of 307 nm was designed by Lee et al. These nanoparticles exhibited significantly higher drug loading (2.6 wt%) and was demonstrated to be better than free ICG on MCF-7 and MDA-MB-231 (mammary adenocarcinoma) cells. Their increased cell killing capability was associated with active targeting [68].

In a different study, ICG-PLGA nanoparticles with a significantly larger size of 817 nm in diameter were utilized by Gomes et al, on P388-D1 (lymphoma) cells. Paired

with 100 J/cm^2 laser irradiation, these nanoparticles were reported to be capable of inducing cell death; albeit less effectively than free ICG at the same concentration [66]. Lesser photocytotoxicity of these nanoparticles could be explained by the lack of active targeting, coupled with larger size which might hamper their cellular uptake. On the contrary, results obtained here suggest that both ICG and ICGNP were equally effective in inducing cell death, with no significant difference observed in cell viability at the same concentrations of ICG and ICGNP.

Most of the previous studies regarding encapsulation of ICG were dual delivery systems, which incorporated chemotherapy or immunotherapy agents as well. Among those studies only a few provide the effects of only encapsulated ICG on the cells. Shen et al. used PLGA nanoparticle co-loaded with DOX and ICG and reported that $20\mu M$ ICG containing nanoparticles caused 24% cell death on EMT-6 (mammary carcinoma) cells upon irradiation (720 J/cm^2), with a total of 96% cell eradication made possible on dual therapy [79]. On RM9 (prostate carcinoma) cells, Lin et al. tested PLGA nanoparticles loaded with both ICG and resiquimod. Almost complete cell eradication was observed at 80 μM ICG-equivalent of nanoparticles, irradiated at 300 J/cm^2 [75]. However, different results obtained by these nanoparticles clarify the need for dosimetry studies targeted to individual cell lines.

4.5 Conclusion

ICGNP produced and characterized in previous part was utilized successfully on PC-3 cells to impart a concentration dependent inhibition of cell viability. Although these nanoparticles were shown to exhibit both photothermal and photodynamic properties; their *in vitro* cell viability inhibition response was found to be majorly due to the thermal effects observed upon laser irradiation.

5. CONCLUSION

Phototherapy is an advantageous treatment modality for cancer owing to its repeatability, minimal collateral damage and minimal invasiveness; yet its efficiency is limited with the light penetration depth. Utilization of NIR photosensitizers is a possible mechanism to increase the targeted depth in tissue however few infrared dye are available. Among these, ICG exhibit promising properties of minimal dark toxicity, suitably energetic triplet state and moderate aqueous solubility, and was previously demonstrated as an effective PDT and PTT agent on various cell lines. Still, it has several shortcomings that needed to be overcome to be useful as a phototherapy agent - a problem that can be addressed with the use of nanosized drug delivery systems. Various DDS incorporating ICG were reported in the literature, yet most of these co-deliver chemotherapy or immunotherapy agents as well, making it hard to distinguish the therapeutic effect of ICG. Most of these studies declare ICG incorporation in these platforms provide photodynamic and photothermal qualities by demonstrating the singlet oxygen production and temperature elevation upon irradiation. Yet, how much of the photocytotoxicity is due to dynamic or thermal mechanisms still needs to be investigated. This study was conducted to encapsulate ICG in PLA nanospheres via a quick and efficient method, to examine its characteristics and to demonstrate its efficiency as a phototherapy agent and tries to ascertain the level of contribution of thermal and dynamic processes in the overall anticancer activity.

PLA was chosen as the carrier polymer due to its safety and biodegradability. Several reports of ICG-encapsulating PLGA nanoparticles and their phototherapeutic effects were present, yet PLA in conjunction with ICG was only used as nanofibers before [98, 99]. As the method of production, nanoprecipitation was utilized in contrast to a double emulsion/solvent evaporation method. Double emulsion/solvent evaporation method is known to provide better loading capacity for hydrophilic drugs at the expense of larger PDI. It also requires larger volumes of toxic solvents to be used and exceptionally energetic emulsification processes to produce nanoparticles. With the

use of nanoprecipitation, which is a simpler process that utilizes marginal amounts of solvents, well-defined nanoparticles with very low PDI were obtained.

Here, PLA nanoparticles produced via nanoprecipitation were used to encapsulate ICG in an attempt to minimize its aggregation and protein binding tendencies. Results from the characterization experiments have shown that ICG could be encapsulated in PLA nanoparticles using nanoprecipitation, albeit at a low loading capacity. This was a direct result of amphiphilic nature of ICG, which causes ICG molecules to quickly partition out of the PLA matrix during nanoparticle production. The resulting nanoparticles exhibited suitable size, morphology and surface charge in order to be used in cell culture experiments. Absorption spectra of ICGNP demonstrated diminished tendency to aggregate with increasing concentrations. Although loading capacity was low, ICGNP suspended in cell culture medium was shown to be capable of producing both singlet oxygen and causing significant heating upon laser irradiation.Therefore ICGNP was deemed suitable to be used in cell culture experiments to test their anticancer effects.

The result of *in vitro* experiments on PC-3 cells suggest that the inhibition of cell viability after laser irradiation was concentration dependent, where ICGNP were as effective as free ICG in decreasing cell viability. At the concentrations tested, no cellular toxicity of ICGNP without laser irradiation was observed. Further investigation revealed that the inhibition of cell viability was the result of photothermal effects dominantly, rather than photodynamic effects, which suggests ICG acted as a chromophore in PLA nanoparticles. Furthermore, ICGNP mediated heating of PC-3 cells was observed to be limited to hyperthermia as final temperatures encountered was around 43 °C, which was also beneficial in providing target cell death without leading to damage in healthy surrounding tissue.

One of the major shortcomings ICGNP was observed to be in loading capacity. As a result of the amphiphilic nature of ICG, dye molecules partitioned out rapidly during nanoparticle formation. Lower loading capacity of nanoparticles necessitated more concentrated nanoparticle suspension to be used in cell culture, potentially in-

ducing dark toxicity at higher ICG-equivalent concentrations. Two possible solutions to this problem has been proposed in the literature: first is the use of a secondary agent (such as chitosan) to bind and increase ICG loading [70], and second is the modification of the polymer itself to covalently attach ICG molecules from which nanoparticles are formed [100]. Covalent attachment of dye to polymer produces more stable nanoparticles with significantly reduced drug release rate however it might also reduce the singlet oxygen production by ICG, thereby limiting its use to only a fluorescent and photothermal agent [101]. Since photothermal mechanisms were observed to be dominant on cell viability inhibition in this study, both methods can be utilized to increase ICG loading without much loss of functionality.

Another important point to improve in this study is the fabrication method. Even though nanoprecipitation is a favorable and extensively studied process, optimization poses a challenge, mainly due to experimental setup. Variables such as solvent phase addition rate should be more controllable and S/NS ratio should be kept constant in an ideal setup. Since addition of the solvent phase would cause an increase in the reaction overall volume, especially at higher S/NS ratios such as 1/2, nanoparticles produced might exhibit more diverse characteristics. Improvement on these points can be provided by utilizing flash nanoprecipitation, in which a fixed mixing volume is used to blend the two phases in considerably shorter mixing times (in the order of milliseconds), producing nanoparticles with tightly controlled size and very low PDI [102].

Active targeting is another possible modification that would improve the efficiency of ICGNP mediated phototherapy. Although nanoparticles with size utilized in this study accumulate in tumors via EPR effect, active targeting would increase the cellular uptake, and in turn the efficiency of phototherapy.

Future work in this topic would primarily focus on increasing ICG loading and surface modification of nanoparticles to provide active targeting to improve intracellular accumulation. With the irradiation regimes used, photothermal action appears to be dominant, therefore focusing on PTT might provide better cell viability inhibition.

This might be done by incorporation of other agents with similar absorption characteristics such as gold nanorods, or by forcing ICG molecules into much stable J-aggregate formation before encapsulation, which would provide better photothermal conversion capability and improved stability of ICG at the expense of diminished singlet oxygen quantum yield [103].

Irradiation control emerges as an important parameter at this point. If PTT were to be utilized as the major mechanism of anticancer action, precise control of temperature elevation would become the most important tool to maximize tumor destruction while minimizing damage to surrounding tissues. One way to achieve this could be the optimization of irradiance regimes. Increasing power density is known to increase the maximum temperature in cells in the presence of ICG, although not as strongly as an increase in ICG concentration [47]. Higher maximum temperature would mean shorter treatment duration, up to 60°C where protein denaturation would begin. Therefore, controlling the rate of temperature elevation as well as the maximum temperature by manipulating laser parameters could prove useful in achieving maximum treatment efficiency.

In conclusion, ICGNP were advantageous in its quick and simple preparation with suitable characteristics, however loading capacity still requires refinement in order to achieve better phototherapeutic effect over a wide range of cell lines. Each component of ICG-mediated phototherapy would benefit from optimization studies to maximize the amount of drug delivered into tissues, to maximize the systemic circulation duration of nanoparticles and to minimize the collateral damage due to uncontrolled heating. Future work can focus both on increasing loading capacity for ICG, which would increase the phototherapeutic efficiency of nanoparticles, and on implementing an active targeting moiety via surface modification, which would improve its cellular uptake.

APPENDIX A. PRELIMINARY STUDIES OF OPTIMIZATION

First attempts at nanoparticle optimization was done with the help of a Box-Behnken design. Box-Behnken is a second-order surface response methodology that is more efficient than central composite and three-level full factorial designs for optimization of parameters. When there are significant interaction between factors, one-factor-at-a-time method could not account for these interactions. Therefore multivariate procedures are used in which all factor levels are changed simultaneously. If the most significant factors are known, optimum conditions can be reached by using complex experimental designs [104, 105]. Among multivariant methods, Box-Behnken is one of the most efficient one for it requires 15 runs for a 3-variable, 3-level design, compared to 20 runs required for central composite.

The important factors for nanoparticle size and loading capacity were determined to be S/NS ratio, PLA concentration and ICG concentration. The levels for these parameters were adapted from the literature for blank PLA nanoparticles and ICG-PLGA nanoparticles. Box-Behnken method requires 3 levels for each factors, namely a high,a low and a middle setting. These settings were summarized in Table A.1.

Table A.1
Factor levels for Box-Behnken Method.

	Low	Middle	High
PLA concentration	5 mg/mL	10 mg/mL	15 mg/ml
ICG concentration	10 μM	30 μM	50 μM
S/NS ratio	0.2	0.4	0.6

Results obtained with this parameter set proved to be unsuitable in terms of size since at 0.6 S/NS ratio, nanoparticle size reached around 500 nm even at low PLA concentration setting. Therefore parameter set was refined for second iteration as seen

in Table A.2 and samples were prepared in three blocks. Optimization was carried out to minimize size and maximize ICG concentration in Minitab 17.

Table A.2
Factor levels for Box-Behnken Method.

	Low	Middle	High
PLA concentration	5 mg/mL	10 mg/mL	15 mg/ml
ICG concentration	10 μM	30 μM	50 μM
S/NS ratio	0.1	0.3	0.5

The results suggested the best possible combination for desired results to be 0.1 S/NS ratio, 50 μM ICG concentration and 11 mg/mL PLA concentration. Nanoparticles produced with these parameters were measured 280 nm in diameter, with a zeta potential of -9 mV. Phototherapeutic effects of these nanoparticles were tested on PC-3 cells, however extreme dark toxicity was encountered. The dark toxicity resulted from over-concentrated nanoparticle suspension due to low loading capacity (around 0.1%).

Some important results obtained from this study were;

1. S/NS ratio had the most significant effect on nanoparticle size
2. ICG concentration had no significant effect on nanoparticle size
3. 15 mg/mL PLA concentration produced significantly larger nanoparticles, while with 5mg/mL, nanoparticle size was significantly smaller but loading capacity was significantly lower as well

The parameter sets for one-factor-at-a-time experiments were constructed using these results as starting points.

APPENDIX B. FT-IR SPECTRA

FT-IR spectra of free ICG, PLA and ICGNP were obtained using ICG and PLA as obtained and ICGNP after lyophilization via FT-IR spectrometer (Perkin Elmer Spectrum Two, MA, USA) equipped with an attenuated total reflectance (ATR) accessory. Samples were scanned between wavenumbers 400-4000 cm^{-1} and constructed as an average of 6 scans. The spectra were presented in Figure B.1.

As the amount of ICG encapsulated in PLA nanospheres were relatively low, its effect on ICGNP spectrum was hard to distinguish. The nanoprecipitation method produces nanoparticles that physically entrap drug molecules, therefore no new band was expected on the ICGNP spectrum. According to the related literature,intensity increase in bands related to ICG (1309 cm^{-1} S=O stretch, 1351 cm^{-1} sulfonate) in ICGNP spectrum confirms that ICG has been incorporated in PLA nanoparticles [99].

Aside from that, several bands related to the aromatic nature of ICG can be observed in ICG spectrum such as aromatic C=C stretches (1400-1500 cm^{-1}) and C-H vinyl stretches (900-1100 cm^{-1}), whose effects can be observed on ICGNP to some extent [97].

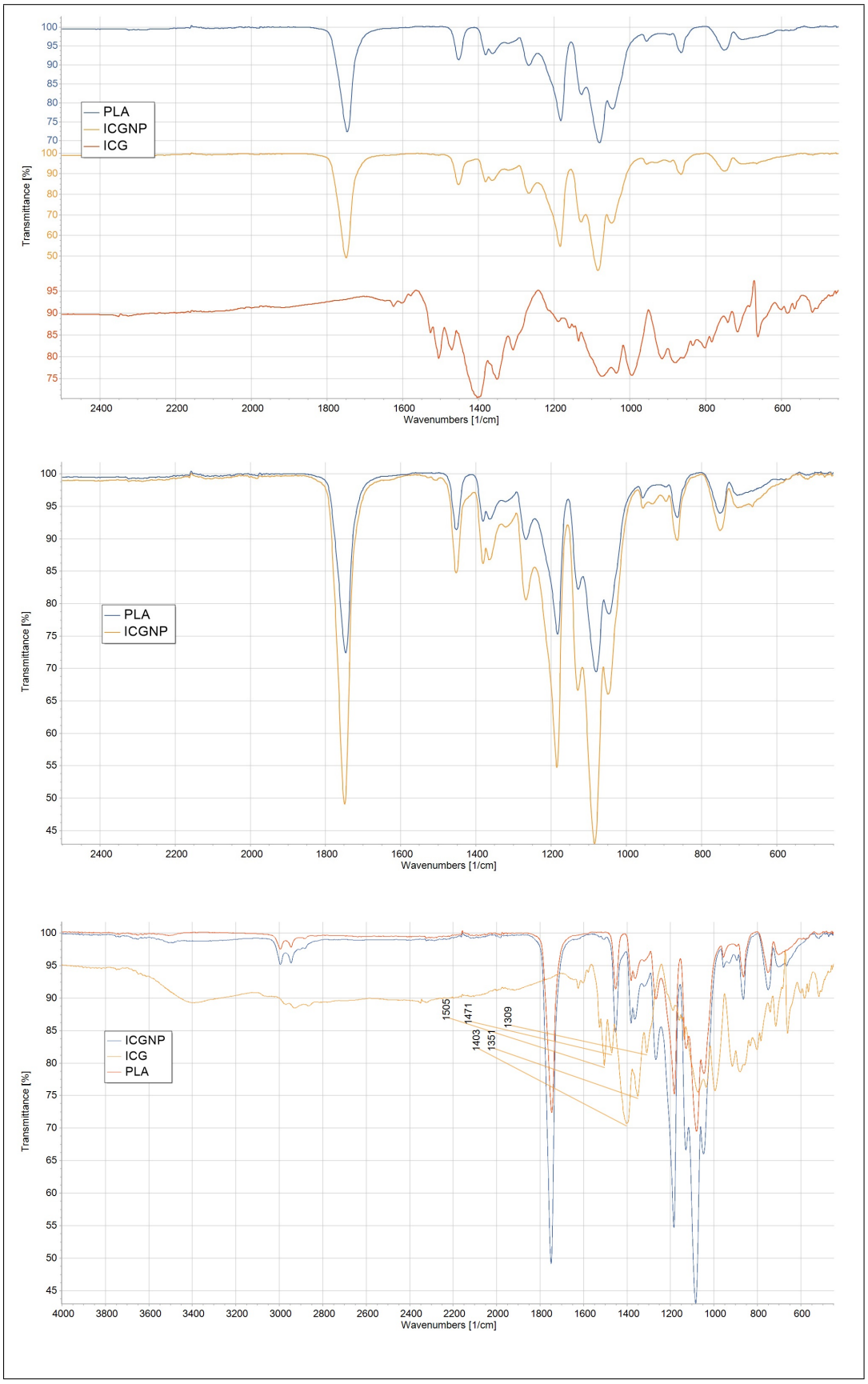

Figure B.1 FT-IR spectra of ICG, PLA and ICGNP.

REFERENCES

1. Shi, H., and P. J. Sadler, "How promising is phototherapy for cancer?," *British Journal of Cancer*, Vol. 123, no. 6, pp. 871–873, 2020.

2. Moan, J., and Q. Peng, "An outline of the hundred-year history of PDT," *Anticancer Research*, Vol. 23, no. 5A, pp. 3591–3600, 2003.

3. Daniell, M. D., and J. S. Hill, "A history of photodynamic therapy," *Australian and New Zealand Journal of Surgery*, Vol. 61, no. 5, pp. 340–348, 1991.

4. Gai, S., G. Yang, P. Yang, F. He, and others., "Recent advances in functional nanomaterials for light–triggered cancer therapy," *Nano Today*, Vol. 19, pp. 146–187, 2018.

5. Sarcan, E. T., M. Silindir-Gunay, and A. Y. Ozer, "Theranostic polymeric nanoparticles for NIR imaging and photodynamic therapy," *International Journal of Pharmaceutics*, Vol. 551, no. 1-2, pp. 329–338, 2018.

6. Master, A., M. Livingston, and A. S. Gupta, "Photodynamic nanomedicine in the treatment of solid tumors: perspectives and challenges," *Journal of Controlled Release*, Vol. 168, no. 1, pp. 88–102, 2013.

7. Tuchin, V. V., E. A. Genina, A. N. Bashkatov, G. V. Simonenko, *et al.*, "A pilot study of ICG laser therapy of acne vulgaris: photodynamic and photothermolysis treatment," *Lasers in Surgery and Medicine: The Official Journal of the American Society for Laser Medicine and Surgery*, Vol. 33, no. 5, pp. 296–310, 2003.

8. Topaloğlu, N., M. Gülsoy, and Ş Yüksel, "Antimicrobial photodynamic therapy of resistant bacterial strains by indocyanine green and 809-nm diode laser," *Photomedicine and Laser Surgery*, Vol. 31, no. 4, pp. 155–162, 2013.

9. Taylor, J. S., J. Zeki, N. Ikegaki, L. Chen, *et al.*, "Combined application of indocyanine green (ICG) and laser lead to targeted tumor cell destruction," *Journal of Pediatric Surgery*, Vol. 53, no. 12, pp. 2475–2479, 2018.

10. Ruhi, M. K., A. Ak, and M. Gülsoy, "Dose-dependent photochemical/photothermal toxicity of indocyanine green-based therapy on three different cancer cell lines," *Photodiagnosis and Photodynamic Therapy*, Vol. 21, pp. 334–343, 2018.

11. Shafirstein, G., W. Bäumler, L. J. Hennings, E. R. Siegel, *et al.*, "Indocyanine green enhanced near-infrared laser treatment of murine mammary carcinoma," *International Journal of Cancer*, Vol. 130, no. 5, pp. 1208–1215, 2012.

12. Fickweiler, S., R. M. Szeimies, W. Bäumler, P. Steinbach, *et al.*, "Indocyanine green: intracellular uptake and phototherapeutic effects in vitro," *Journal of Photochemistry and Photobiology B: biology*, Vol. 38, no. 2-3, pp. 178–183, 1997.

13. Lim, H. J., and C. H. Oh, "Indocyanine green-based photodynamic therapy with 785 nm light emitting diode for oral squamous cancer cells," *Photodiagnosis and Photodynamic Therapy*, Vol. 8, no. 4, pp. 337–342, 2011.

14. Abels, C., S. Fickweiler, P. Weiderer, W. Bäumler, *et al.*, "Indocyanine green (ICG) and laser irradiation induce photooxidation," *Archives of Dermatological Research*, Vol. 292, no. 8, pp. 404–411, 2000.

15. Bozkulak, Ö., R. F. Yamaci, Ö. Tabakoğlu, and M. Gülsoy, "Photo-toxic effects of 809-nm diode laser and indocyanine green on MDA-MB231 breast cancer cells," *Photodiagnosis and Photodynamic Therapy*, Vol. 6, no. 2, pp. 117–121, 2009.

16. Bäumler, W., C. Abels, S. Karrer, T. Weiss, *et al.*, "Photo-oxidative killing of human colonic cancer cells using indocyanine green and infrared light," *British Journal of Cancer*, Vol. 80, no. 3, pp. 360–363, 1999.

17. Giraudeau, C., A. Moussaron, A. Stallivieri, S. Mordon, and S. Frochot, "Indocyanine green: photosensitizer or chromophore? Still a debate," *Current Medicinal Chemistry*, Vol. 21, no. 16, pp. 1871–1897, 2014.

18. Saxena, V., M. Sadoqi, and J. Shao, "Degradation kinetics of indocyanine green in aqueous solution," *Journal of Pharmaceutical Sciences*, Vol. 92, no. 10, pp. 2090–2097, 2003.

19. Engel, E., R. Schraml, T. Maisch, K. Kobuch, *et al.*, "Light-induced decomposition of indocyanine green," *Investigative Ophthalmology & Visual Science*, Vol. 49, no. 5, pp. 1777–1783, 2008.

20. R Weigand, F Rotermund, A. P., "Aggregation dependent absorption reduction of indocyanine green," *The Journal of Physical Chemistry A*, Vol. 101, no. 42, pp. 7729–7734, 1997.

21. Landsman, M. L., G. Kwant, G. A. Mook, and W. G. Zijlstra, "Light-absorbing properties, stability, and spectral stabilization of indocyanine green," *Journal of Applied Physiology*, Vol. 40, no. 4, pp. 575–583, 1976.

22. Holzer, W., M. Mauerer, A. Penzkofer, R. M. Szeimies, *et al.*, "Photostability and thermal stability of indocyanine green," *Journal of Photochemistry and Photobiology B: Biology*, Vol. 47, no. 2-3, pp. 155–164, 1998.

23. Mindt, S., I. Karampinis, M. John, M. Neumaier, *et al.*, "Stability and degradation of indocyanine green in plasma, aqueous solution and whole blood," *Photochemical & Photobiological Sciences*, Vol. 17, no. 9, pp. 1189–1196, 2018.

24. Nezza, F. D., G. Guerra, C. Costagliola, L. Zeppa, *et al.*, "Thermodynamic properties and photodegradation kinetics of indocyanine green in aqueous solution," *Dyes and Pigments*, Vol. 134, pp. 342–347, 2016.

25. Philip, R., A. Penzkofer, W. Bäumler, R. M. Szeimies, *et al.*, "Absorption and fluorescence spectroscopic investigation of indocyanine green," *Journal of Photochemistry and Photobiology A: Chemistry*, Vol. 96, no. 1-3, pp. 137–148, 1996.

26. Xie, Z., T. Fan, J. An, W. Choi, *et al.*, "Emerging combination strategies with phototherapy in cancer nanomedicine," *Chemical Society Reviews*, Vol. 49, no. 22, pp. 8065–8087, 2020.

27. Correia, J. H., J. A. Rodrigues, S. Pimenta, T. Dong, *et al.*, "Photodynamic therapy review: principles, photosensitizers, applications, and future directions," *Pharmaceutics*, Vol. 13, no. 9, p. 1332, 2021.

28. Zhu, T. C., and J. C. Finlay, "The role of photodynamic therapy (PDT) physics," *Medical Physics*, Vol. 35, no. 7Part1, pp. 3127–3136, 2008.

29. Kashyap, A., E. Ramasamy, V. Ramalingam, and M. Pattabiraman, "Supramolecular control of singlet oxygen generation," *Molecules*, Vol. 26, no. 9, p. 2673, 2021.

30. Allemann, I. B., and J. Kaufman, "Laser principles," in *Basics in Dermatological Laser Applications*, Vol. 42, pp. 7–23, Karger Publishers, 2011.

31. Castano, A. P., T. N. Demidova, and M. R. Hamblin, "Mechanisms in photodynamic therapy: part one - photosensitizers, photochemistry and cellular localization," *Photodiagnosis and Photodynamic Therapy*, Vol. 1, no. 4, pp. 279–293, 2004.

32. DeRosa, M. C., and R. J. Crutchley, "Photosensitized singlet oxygen and its applications," *Coordination Chemistry Reviews*, Vol. 233, pp. 351–371, 2002.

33. Josefsen, L. B., and R. W. Boyle, "Photodynamic therapy and the development of metal-based photosensitisers," *Metal-based Drugs*, Vol. 2008, 2008.

34. Fekrazad, R., A. Nejat, and K. A. M. Kalhori, "Antimicrobial photodynamic therapy with nanoparticles versus conventional photosensitizer in oral diseases," in *Nanostructures for Antimicrobial Therapy*, pp. 237–259, Elsevier, 2017.

35. Kadkhoda, J., A. Tarighatnia, J. Barar, A. Aghanejad, *et al.*, "Recent advances and trends in nanoparticles based photothermal and photodynamic therapy," *Photodiagnosis and Photodynamic Therapy*, p. 102697, 2021.

36. Hatz, S., J. D. C. Lambert, and P. R. Ogilby, "Measuring the lifetime of singlet oxygen in a single cell: addressing the issue of cell viability," *Photochemical & Photobiological Sciences*, Vol. 6, no. 10, pp. 1106–1116, 2007.

37. Doughty, A. C. V., A. R. Hoover, E. Layton, C. K. Murray, *et al.*, "Nanomaterial applications in photothermal therapy for cancer," *Materials*, Vol. 12, no. 5, p. 779, 2019.

38. Shibu, E. S., M. Hamada, N. Murase, and V. Biju, "Nanomaterials formulations for photothermal and photodynamic therapy of cancer," *Journal of Photochemistry and Photobiology C: Photochemistry Reviews*, Vol. 15, pp. 53–72, 2013.

39. Zhao, L., X. Zhang, X. Wang, X. Guan, *et al.*, "Recent advances in selective photothermal therapy of tumor," *Journal of Nanobiotechnology*, Vol. 19, no. 1, pp. 1–15, 2021.

40. Zheng, M., C. Yue, Y. Ma, P. Gong, *et al.*, "Single-step assembly of DOX/ICG loaded lipid–polymer nanoparticles for highly effective chemo-photothermal combination therapy," *ACS Nano*, Vol. 7, no. 3, pp. 2056–2067, 2013.

41. Sigma-Aldrich, *Cardiogreen*, 2022. Available: https://www.sigmaaldrich.com.

42. Prahl, S., *Optical Absorption of Indocyanine Green (ICG)*, 2018. Available: https://omlc.org/spectra/icg/.

43. Yu, J., M. A. Yaseen, B. Anvari, and M. S. Wong, "Synthesis of near-infrared-absorbing nanoparticle-assembled capsules," *Chemistry of Materials*, Vol. 19, no. 6, pp. 1277–1284, 2007.

44. Prahl, S., *Tabulated Molar Extinction Coefficient for Methylene Blue in Water*, 1998. Available: https://omlc.org/spectra/mb/mb-water.html.

45. Tovar, J. S. D., G. Kassab, N. M. Inada, V. S. Bagnato, *et al.*, "Photodegradation in the infrared region of indocyanine green in aqueous solution," in *2019 SBFoton International Optics and Photonics Conference (SBFoton IOPC)*, pp. 1–5, IEEE, 2019.

46. Reindl, S., A. Penzkofer, S. H. Gong, M. Landthaler, *et al.*, "Quantum yield of triplet formation for indocyanine green," *Journal of Photochemistry and Photobiology A: Chemistry*, Vol. 105, no. 1, pp. 65–68, 1997.

47. Long, S., Y. Xu, F. Zhou, B. Wang, *et al.*, "Characteristics of temperature changes in photothermal therapy induced by combined application of indocyanine green and laser," *Oncology Letters*, Vol. 17, no. 4, pp. 3952–3959, 2019.

48. Uchegbu, I. F., and A. G. Schatzlein, *Polymers in Drug Delivery*, CRC Press, 2006.

49. Gaumet, M., A. Vargas, R. Gurny, and F. Delie, "Nanoparticles for drug delivery: the need for precision in reporting particle size parameters," *European Journal of Pharmaceutics and Biopharmaceutics*, Vol. 69, no. 1, pp. 1–9, 2008.

50. Greish, K., "Enhanced permeability and retention (EPR) effect for anticancer nanomedicine drug targeting," in *Cancer Nanotechnology*, pp. 25–37, Springer, 2010.

51. Dwivedi, P., K. M. Karumbaiah, and R. Das, "Nano-size polymers via precipitation of polymer solutions," in *Nano-Size Polymers*, pp. 251–282, Springer, 2016.

52. Anderson, J. M., and M. S. Shive, "Biodegradation and biocompatibility of PLA and PLGA microspheres," *Advanced Drug Delivery Reviews*, Vol. 28, no. 1, pp. 5–24, 1997.

53. Asad, M. I., N. Ahmed, A. Ur-Rehman, and G. M. Khan, "Polylactide: the polymer revolutionizing the biomedical field," in *Materials for Biomedical Engineering*, pp. 381–415, Elsevier, 2019.

54. Tyler, B., D. Gullotti, A. Mangraviti, T. Utsuki, *et al.*, "Polylactic acid (PLA) controlled delivery carriers for biomedical applications," *Advanced Drug Delivery Reviews*, Vol. 107, pp. 163–175, 2016.

55. Hornig, S., T. Heinze, C. R. Becer, and U. S. Schubert, "Synthetic polymeric nanoparticles by nanoprecipitation," *Journal of Materials Chemistry*, Vol. 19, no. 23, pp. 3838–3840, 2009.

56. Lassalle, V., and M. L. Ferreira, "PLA nano-and microparticles for drug delivery: an overview of the methods of preparation," *Macromolecular Bioscience*, Vol. 7, no. 6, pp. 767–783, 2007.

57. Nagavarma, B. V. N., H. K. S. Yadav, A. V. L. S. Ayaz, L. S. Vasudha, *et al.*, "Different techniques for preparation of polymeric nanoparticles-a review," *Asian Journal of Pharmaceutical and Clinical Research*, Vol. 5, no. 3, pp. 16–23, 2012.

58. Rao, J. P., and K. E. Geckeler, "Polymer nanoparticles: preparation techniques and size-control parameters," *Progress in Polymer Science*, Vol. 36, no. 7, pp. 887–913, 2011.

59. Maharana, T., B. Mohanty, and Y. S. Negi, "Preparation of poly (lactic acid) nanoparticles and optimization of the particle size," *International Journal of Green Nanotechnology: Physics and Chemistry*, Vol. 2, no. 2, pp. P100–P109, 2010.

60. Jeffery, H., S. S. Davis, and D. T. O'hagan, "The preparation and characterisation of poly (lactide-co-glycolide) microparticles. I: Oil-in-water emulsion solvent evaporation," *International Journal of Pharmaceutics*, Vol. 77, no. 2-3, pp. 169–175, 1991.

61. Chorny, M., I. Fishbein, H. D. Danenberg, and G. Golomb, "Lipophilic drug loaded nanospheres prepared by nanoprecipitation: effect of formulation variables on size, drug recovery and release kinetics," *Journal of Controlled Release*, Vol. 83, no. 3, pp. 389–400, 2002.

62. Legrand, P., S. Lesieur, A. Bochot, R. Gref, *et al.*, "Influence of polymer behaviour in organic solution on the production of polylactide nanoparticles by nanoprecipitation," *International Journal of Pharmaceutics*, Vol. 344, no. 1-2, pp. 33–43, 2007.

63. Porcu, E. P., A. Salis, E. Gavini, G. Rassu, *et al.*, "Indocyanine green delivery systems for tumour detection and treatments," *Biotechnology Advances*, Vol. 34, no. 5, pp. 768–789, 2016.

64. Saxena, V., M. Sadoqi, and J. Shao, "Indocyanine green-loaded biodegradable nanoparticles: preparation, physicochemical characterization and in vitro release," *International Journal of Pharmaceutics*, Vol. 278, no. 2, pp. 293–301, 2004.

65. Saxena, V., M. Sadoqi, and J. Shao, "Enhanced photo-stability, thermal-stability and aqueous-stability of indocyanine green in polymeric nanoparticulate systems," *Journal of Photochemistry and Photobiology B: Biology*, Vol. 74, no. 1, pp. 29–38, 2004.

66. Gomes, A. J., L. O. Lunardi, J. M. Marchetti, C. N. Lunardi, *et al.*, "Indocyanine green nanoparticles useful for photomedicine," *Photomedicine and Laser Therapy*, Vol. 24, no. 4, pp. 514–521, 2006.

67. Patel, R. H., A. S. Wadajkar, N. L. Patel, V. C. Kavuri, *et al.*, "Multifunctionality of indocyanine green-loaded biodegradable nanoparticles for enhanced optical imaging and hyperthermia intervention of cancer," *Journal of Biomedical Optics*, Vol. 17, no. 4, p. 046003, 2012.

68. Lee, Y. H., and Y. H. Lai, "Synthesis, characterization, and biological evaluation of anti-HER2 indocyanine green-encapsulated PEG-coated PLGA nanoparticles for targeted phototherapy of breast cancer cells," *PLoS One*, Vol. 11, no. 12, p. e0168192, 2016.

69. Zhao, P., M. Zheng, C. Yue, Z. Luo, *et al.*, "Improving drug accumulation and photothermal efficacy in tumor depending on size of ICG loaded lipid-polymer nanoparticles," *Biomaterials*, Vol. 35, no. 23, pp. 6037–6046, 2014.

70. Sánchez-Ramírez, D. R., R. Domínguez-Ríos, J. Juárez, M. Valdés, *et al.*, "Biodegradable photoresponsive nanoparticles for chemo-, photothermal-and photodynamic therapy of ovarian cancer," *Materials Science and Engineering: C*, Vol. 116, p. 111196, 2020.

71. Srinivasan, S., R. Manchanda, T. Lei, A. Nagesetti, *et al.*, "Targeted nanoparticles for simultaneous delivery of chemotherapeutic and hyperthermia agents–an in vitro study," *Journal of Photochemistry and Photobiology B: Biology*, Vol. 136, pp. 81–90, 2014.

72. Tang, Y., T. Lei, R. Manchanda, A. Nagesetti, *et al.*, "Simultaneous delivery of chemotherapeutic and thermal-optical agents to cancer cells by a polymeric (PLGA) nanocarrier: an in vitro study," *Pharmaceutical Research*, Vol. 27, no. 10, pp. 2242–2253, 2010.

73. Manchanda, R., A. Fernandez-Fernandez, A. Nagesetti, and A. J. McGoron, "Preparation and characterization of a polymeric (PLGA) nanoparticulate drug delivery system with simultaneous incorporation of chemotherapeutic and thermo-optical agents," *Colloids and Surfaces B: Biointerfaces*, Vol. 75, no. 1, pp. 260–267, 2010.

74. Wu, H., C. You, F. Chen, J. Jiao, *et al.*, "Enhanced cellular uptake of near-infrared triggered targeted nanoparticles by cell-penetrating peptide TAT for combined chemo/photothermal/photodynamic therapy," *Materials Science and Engineering: C*, Vol. 103, p. 109738, 2019.

75. Lin, W., C. Li, N. Xu, M. Watanabe, *et al.*, "Dual-functional PLGA nanoparticles co-loaded with indocyanine green and resiquimod for prostate cancer treatment," *International Journal of Nanomedicine*, Vol. 16, p. 2775, 2021.

76. Xu, L., S. B. Wang, C. Xu, D. Han, *et al.*, "Multifunctional albumin-based delivery system generated by programmed assembly for tumor-targeted multimodal therapy and imaging," *ACS Applied Materials & Interfaces*, Vol. 11, no. 42, pp. 38385–38394, 2019.

77. Kim, S. S., H. K. Kim, H. Kim, W. T. Lee, *et al.*, "Hyperthermal paclitaxel-bound albumin nanoparticles co-loaded with indocyanine green and hyaluronidase for treating pancreatic cancers," *Archives of Pharmacal Research*, Vol. 44, no. 2, pp. 182–193, 2021.

78. Pham, P. T. T., X. T. Le, H. Kim, H. K. Kim, *et al.*, "Indocyanine green and curcumin co-loaded nano-fireball-like albumin nanoparticles based on near-infrared-induced hyperthermia for tumor ablation," *International Journal of Nanomedicine*, Vol. 15, p. 6469, 2020.

79. Shen, X., T. Li, Z. Chen, X. Xie, *et al.*, "NIR-light-triggered anticancer strategy for dual-modality imaging-guided combination therapy via a bioinspired hybrid PLGA nanoplatform," *Molecular Pharmaceutics*, Vol. 16, no. 3, pp. 1367–1384, 2019.

80. Saxena, V., M. Sadoqi, S. Kumar, and J. Shao, "Long-circulating near-infrared fluorescent nanoparticles for diagnosis and photodynamic therapy of cutaneous cancers," in *Lasers in Surgery: Advanced Characterization, Therapeutics, and Systems XIV*, Vol. 5312, pp. 41–46, International Society for Optics and Photonics, 2004.

81. Aghda, N. H., S. M. Abdulsahib, C. Severson, E. J. Lara, *et al.*, "Induction of immunogenic cell death of cancer cells through nanoparticle-mediated dual chemotherapy and photothermal therapy," *International Journal of Pharmaceutics*, Vol. 589, p. 119787, 2020.

82. Hao, Y., L. Wang, Y. Zhao, D. Meng, *et al.*, "Targeted imaging and chemo-phototherapy of brain cancer by a multifunctional drug delivery system," *Macromolecular Bioscience*, Vol. 15, no. 11, pp. 1571–1585, 2015.

83. McClean, S., E. Prosser, E. Meehan, D. O'Malley, *et al.*, "Binding and uptake of biodegradable poly-DL-lactide micro-and nanoparticles in intestinal epithelia," *European Journal of Pharmaceutical Sciences*, Vol. 6, no. 2, pp. 153–163, 1998.

84. Tang, L., X. Yang, Q. Yin, K. Cai, *et al.*, "Investigating the optimal size of anticancer nanomedicine," *Proceedings of the National Academy of Sciences*, Vol. 111, no. 43, pp. 15344–15349, 2014.

85. Gref, R., P. Couvreur, G. Barratt, and E. Mysiakine, "Surface-engineered nanoparticles for multiple ligand coupling," *Biomaterials*, Vol. 24, no. 24, pp. 4529–4537, 2003.

86. Guhagarkar, S. A., V. C. Malshe, and P. V. Devarajan, "Nanoparticles of polyethylene sebacate: a new biodegradable polymer," *Aaps Pharmscitech*, Vol. 10, no. 3, pp. 935–942, 2009.

87. Miladi, K., S. Sfar, H. Fessi, and A. Elaissari, "Nanoprecipitation process: from particle preparation to in vivo applications," in *Polymer Nanoparticles for Nanomedicines*, pp. 17–53, Springer, 2016.

88. Zambaux, M. F., F. Bonneaux, R. Gref, P. Maincent, *et al.*, "Influence of experimental parameters on the characteristics of poly (lactic acid) nanoparticles prepared by a double emulsion method," *Journal of Controlled Release*, Vol. 50, no. 1-3, pp. 31–40, 1998.

89. Varenne, F., A. Makky, M. Gaucher-Delmas, F. Violleau, *et al.*, "Multimodal dispersion of nanoparticles: a comprehensive evaluation of size distribution with 9 size measurement methods," *Pharmaceutical Research*, Vol. 33, no. 5, pp. 1220–1234, 2016.

90. Leo, E., B. Brina, F. Forni, and M. A. Vandelli, "In vitro evaluation of PLA nanoparticles containing a lipophilic drug in water-soluble or insoluble form," *International Journal of Pharmaceutics*, Vol. 278, no. 1, pp. 133–141, 2004.

91. Mitchell, M. J., M. M. Billingsley, R. M. Haley, M. E. Wechsler, *et al.*, "Engineering precision nanoparticles for drug delivery," *Nature Reviews Drug Discovery*, Vol. 20, no. 2, pp. 101–124, 2021.

92. Lee, Y. H., and D. S. Chang, "Fabrication, characterization, and biological evaluation of anti-HER2 indocyanine green-doxorubicin-encapsulated PEG-b-PLGA copolymeric nanoparticles for targeted photochemotherapy of breast cancer cells," *Scientific Reports*, Vol. 7, no. 1, pp. 1–13, 2017.

93. Chen, H. H., I. L. Lu, T. I. Liu, Y. C. Tsai, *et al.*, "Indocyanine green/doxorubicin-encapsulated functionalized nanoparticles for effective combination therapy against human MDR breast cancer," *Colloids and Surfaces B: Biointerfaces*, Vol. 177, pp. 294–305, 2019.

94. Tang, Y., and A. J. McGoron, "Combined effects of laser-ICG photothermotherapy and doxorubicin chemotherapy on ovarian cancer cells," *Journal of Photochemistry and Photobiology B: Biology*, Vol. 97, no. 3, pp. 138–144, 2009.

95. Ting, C. W., Y. H. Chou, S. Y. Huang, and W. H. Chiang, "Indocyanine green-carrying polymeric nanoparticles with acid-triggered detachable PEG coating and drug release for boosting cancer photothermal therapy," *Colloids and Surfaces B: Biointerfaces*, Vol. 208, p. 112048, 2021.

96. Nomura, S., Y. Morimoto, H. Tsujimoto, M. Arake, *et al.*, "Highly reliable, targeted photothermal cancer therapy combined with thermal dosimetry using a near-infrared absorbent," *Scientific Reports*, Vol. 10, no. 1, pp. 1–7, 2020.

97. Lee, E. H., M. K. Lee, and S. J. Lim, "Enhanced stability of indocyanine green by encapsulation in zein-phosphatidylcholine hybrid nanoparticles for use in the phototherapy of cancer," *Pharmaceutics*, Vol. 13, no. 3, p. 305, 2021.

98. Preis, E., T. Anders, J. Širc, R. Hobzova, *et al.*, "Biocompatible indocyanine green loaded PLA nanofibers for in situ antimicrobial photodynamic therapy," *Materials Science and Engineering: C*, Vol. 115, p. 111068, 2020.

99. Ege, Z. R., A. Akan, F. N. Oktar, C. Lin, *et al.*, "Encapsulation of indocyanine green in poly (lactic acid) nanofibers for using as a nanoprobe in biomedical diagnostics," *Materials Letters*, Vol. 228, pp. 148–151, 2018.

100. Machado, M. G. C., G. Pound-Lana, M. A. de Oliveira, E. G. Lanna, *et al.*, "Labeling PLA-PEG nanocarriers with IR780: physical entrapment versus covalent attachment to polylactide," *Drug Delivery and Translational Research*, Vol. 10, no. 6, pp. 1626–1643, 2020.

101. Xin, Y., T. Liu, and C. Yang, "Development of PLGA-lipid nanoparticles with covalently conjugated indocyanine green as a versatile nanoplatform for tumor-targeted imaging and drug delivery," *International Journal of Nanomedicine*, Vol. 11, p. 5807, 2016.

102. Saad, W. S., and R. K. Prud'homme, "Principles of nanoparticle formation by flash nanoprecipitation," *Nano Today*, Vol. 11, no. 2, pp. 212–227, 2016.

103. Liu, R., J. Tang, Y. Xu, Y. Zhou, *et al.*, "Nano-sized indocyanine green J-aggregate as a one-component theranostic agent," *Nanotheranostics*, Vol. 1, no. 4, p. 430, 2017.

104. Tekindal, M. A., H. Bayrak, B. Özkaya, and Y. Genç, "Box-Behnken experimental design in factorial experiments: the importance of bread for nutrition and health running head," *Turkish Journal of Field Crops*, Vol. 17, no. 2, pp. 115–123, 2012.

105. Ferreira, S. L. C., R. E. Bruns, H. S. Ferreira, G. D. Matos, *et al.*, "Box-Behnken design: an alternative for the optimization of analytical methods," *Analytica Chimica Acta*, Vol. 597, no. 2, pp. 179–186, 2007.